Type 2 Diabetes: One Disease, Many Pathways

Joon Ha

Arthur Sherman

Laboratory of Biological Modeling

National Institutes of Health

Bethesda, MD USA

Abstract (248 words)

Diabetes is a chronic, progressive disease that calls for longitudinal data and analysis. We introduce a longitudinal mathematical model that is capable of representing the metabolic state of an individual at any point in time during their progression from normal glucose tolerance to type 2 diabetes (T2D) over a period of years. As an application of the model, we account for the diversity of pathways typically followed, focusing on two extreme alternatives, one that goes through impaired fasting glucose (IFG) first, and one that goes through impaired glucose tolerance (IGT) first. These two pathways are widely recognized to stem from distinct metabolic abnormalities in hepatic glucose production and peripheral glucose uptake, respectively. We confirm this but go beyond to show that IFG and IGT lie on a continuum ranging from high hepatic insulin resistance and low peripheral insulin resistance to low hepatic resistance and high peripheral resistance. We show that IFG generally incurs IGT, and IGT generally incurs IFG on the way to T2D, highlighting the difference between innate and acquired defects and the need to assess patients early to determine their underlying primary impairment. We illustrate the relevance of this for patient stratification by simulating the effects of properly and improperly targeted therapies. The model also incorporates insulin granule exocytosis and accounts for both first and second phase secretion. Simulations suggest that the loss of first phase secretion in both the IGT-first and IFG-first pathways is only a marker of progression to diabetes, not a causative mechanism.

Introduction

Diabetes is by definition a state of hyperglycemia, but its natural history is diverse. For example, some individuals experience fasting hyperglycemia first (Impaired Fasting Glucose, IFG), followed by hyperglycemia at the two-hour time point (2hPG) of an oral glucose tolerance test (OGTT), defined as Impaired Glucose Tolerance (IGT), and some experience these in the opposite order. Eventually, all people with diabetes will have both IFG and IGT (combined glucose impairment, CGI), so we refer to these two pathways as "IGT-first" and "IFG-first", respectively. An important implication of these observations is that the best period for determining differences in the underlying physiology of these pathways is during the pre-diabetic stage, when the phenotypes are still distinct.

Prediabetes is also the stage in which progression to type 2 diabetes (T2D) can be markedly delayed or prevented [1], and interventions can plausibly be made even more effective by targeting the specific metabolic defects of the patient. For example, IFG is generally thought to reflect insulin resistance at the liver, resulting in elevated hepatic glucose production (HGP), whereas IGT is thought to reflect peripheral insulin resistance, mainly in muscle, resulting in reduced glucose disposal. One would like to know whether using drugs that primarily affect hepatic or peripheral insulin resistance makes a material difference for patients on the IFG-first or IGT-first pathways, and whether any such benefit carries over once T2D has begun.

Moreover, diabetes is not a state that one enters and exits, like an infection, but a chronic condition that is the culmination of a series of gradual changes. Understanding of this progression is best obtained by longitudinal studies over a period of years or decades. Here we will focus on one such study, the Baltimore Longitudinal Study of Aging (BLSA) [2], which asked whether CGI is an obligatory stage between IFG and T2D and between IGT and T2D (Fig. A1).

These features of diabetes suggest that a longitudinal mathematical model for disease progression could be a valuable adjunct to clinical studies. Here we establish such a model and demonstrate that it can distinguish hepatic and peripheral insulin resistance and can simulate the IGT-first and IFG-first pathways to T2D over a period of years. We will use the model to address the clinical questions raised by the BLSA and Perrault studies. By tracking virtual patients continuously in time, the model can interpolate between clinical observations, which are necessarily sparsely sampled, and indicate what is likely to have happened in the interim.

The model provides broader insight into the different insulin-resistance phenotypes, showing that a wide array of pathways, ranging from isolated IFG to isolated IGT to combinations of the two, can be obtained by combining different degrees of hepatic and peripheral insulin resistance. Thus, the apparent clinical diversity of individual paths comprises a set of quantitative variants within a unified process of metabolic dysfunction.

There is also diversity in the relative contributions of insulin resistance and beta-cell dysfunction to diabetes pathogenesis. This is particularly apparent in comparing diabetes risk factors in populations with a high prevalence of obesity, such as those of African descent and Native Americans, to populations in which diabetes risk is seen among lean individuals and beta-cell function is weaker, such as South and East Asians; populations of European descent tend to lie in between [3]. Furthermore, beta-cell dysfunction can be subdivided into defects in first- and second-phase insulin secretion. As a first installment on this large and complex set of problems, we examine whether the loss of first-phase secretion early in pre-diabetes plays a fundamental causal role in T2D development or is just a useful marker.

General modeling approach

The diabetes field is fortunate to have a strong tradition of mathematical modeling [4,5]. A common feature of those models is that they provide snapshots in time of the metabolic state of an individual, including insulin resistance and beta-cell function. These models have been used to track progression by taking a series of snapshots, but they do not contain mechanisms of progression and do not describe trajectories of progression.

The model developed here belongs to a different family of models that seek to explain disease progression mechanistically, rather than assess the current state. It is an extension of our previously published model of beta-cell mass and function, which successfully simulated progression to diabetes in rodents over months and humans over years [6]. That model, in turn, was based on the seminal model of [7], which expressed mathematically the hypothesis that beta-cell mass provides negative feedback on a slow time scale to compensate for insulin resistance. If that compensation is inadequate, however, the toxic effects of very high glucose overcome the stimulatory effects of moderately elevated glucose. The normal homeostatic negative feedback is converted to positive feedback, leading to deterioration in glucose tolerance and culminating in diabetes. This fundamental concept has been incorporated into other models that broadly agree but emphasize different details [8–13]. Notably, the model of [9] was shown to be able to account for the progression of fasting hyperglycemia and T2D observed in the Diabetes Prevention Program (DPP) [1].

A third class of modeling studies has fit longitudinal data from clinical studies with non-linear mixed effects statistical approaches to assess the magnitude of treatment effects on glucose, insulin and HbA1c [14,15] or, by fitting to a modified form of the model of [7], on beta-cell mass and insulin sensitivity [16]. See [13] for further comment on the models cited here and other models, and see [17] for a perspective on modeling T2D.

The initial wave of mechanistic longitudinal models simulated fasting or average daily glucose and were therefore unable to describe post-prandial responses or responses to glucose challenges such as OGTTs

and IVGTTs. A recent model [13] added the capability of following daily and post-challenge glucose variations and was fit to OGTT data from the DPP. It also introduced a distinction between peripheral and hepatic insulin resistance in order to account for the effects of drug and lifestyle interventions on these parameters.

We also, using a different methodology, introduce simulations of OGTTs at selected points during progression, and separate representations for hepatic and peripheral insulin resistance. We use these new features to differentiate progression by either 2hPG or FPG. We perform IVGTTs as well to illustrate the evolution of the acute insulin response to glucose (AIRg), often used to assess beta-cell function. This requires the model to simulate first and second phase secretion, which we accomplish by incorporating a previously published model for insulin granule exocytosis [18].

This study focuses on mechanism and insight, rather than assessment. Instead of fitting parameters to particular data sets, we assume parameters and investigate the trajectories of glycemia and insulin secretion that result. We demonstrate that the model captures known features of diabetes pathogenesis data and provides novel insights and interpretations of the data. We conceptualize this as building a factory, not a product. Once the utility of the model is established, we expect that a wide variety of applications to clinical data will become possible.

Materials and Methods

We briefly review the previous version of the model [6] and then describe the enhancements introduced here. The enhanced version has been used to study clinical implications of differences in glucose time courses during an OGTT [19], but was not documented in detail. Parameter values and details of functions not given here are in the Appendix.

Previous version of the model

The core element, retained in the new version, is a glucose-insulin feedback loop, represented by two differential equations adapted from the Minimal Model of Bergman and Cobelli [20] as modified in [7]:

$$\frac{dG}{dt} = MEAL + HGP - (E_{GO} + S_I I)G \quad (1)$$

$$\frac{dI}{dt} = \frac{\beta}{V} ISR - kI \quad (2)$$

The glucose (G) equation (Eq. 1) says that G increases on a time scale of hours as a result of meal influx and hepatic glucose production (HGP) and decreases as a result of uptake, which has both insulin-independent and insulin-dependent components. The factor S_I in the insulin-dependent term is closely related to the well-known sensitivity to insulin reported by the Minimal Model. The insulin (I) equation (Eq. 2) says that I decreases due to removal, mainly in the liver, with rate constant k, and increases due to secretion by beta cells, where β is the beta-cell mass, ISR is the insulin secretion rate per unit mass, and V is the volume of distribution. In the original version, ISR depended only on G, through the rate of beta-cell metabolism M:

$$ISR = \sigma \frac{(M+\gamma)^{kISR}}{\alpha_{ISR}^{kISR} + (M+\gamma)^{kISR}} \quad (3)$$

where M was assumed to be a sigmoidally-increasing function of G:

$$M = \frac{G^{kM}}{\alpha_M^{kM} + G^{kM}} \quad (4)$$

The parameter γ in Eq. (3) represents the effect of K(ATP) channel density to shift the glucose dependence of secretion (the triggering pathway [21]); when the channel density is low, γ is high, and shifts the dependence to the left, increasing secretion for the same level of M because Ca^{2+} is higher. Experiments in [22] showed that mouse beta cells in vitro adjust the K(ATP) channel density down in response to sustained (overnight) elevated glucose. This has also been observed in vivo in humans [23–25], along with evidence of reduced insulin clearance, k, (19–21) which we omit here for simplicity. This can be viewed as the first line of defense through enhanced beta-cell function against insulin resistance over a time scale of days (e.g. holiday overeating).

153 The value of γ depends on glucose, which is taken into account by adding a third differential equation to
154 the system:

155 $$\frac{d\gamma}{dt} = \frac{\gamma_\infty(G)-\gamma}{\tau_\gamma} \quad (5)$$

156

157 where γ_∞ is an increasing sigmoidal function of G, and τ_γ is the time constant.

158 Insulin resistance that persists over longer periods (months in humans) despite reduced K(ATP) channel
159 density, is assumed to trigger a further level of compensatory increased beta-cell function via σ, the
160 maximal insulin secretion capacity (Eq. 3). This corresponds to the amplifying effects of metabolism
161 and/or modulators such as GLP-1 and ACh on the efficacy of Ca^{2+} to drive insulin granule exocytosis.
162 This second aspect of beta-cell functional compensation entails a fourth differential equation:

163 $$\frac{d\sigma}{dt} = \frac{\sigma_\infty(ISR,M)-\sigma}{\tau_\sigma} \quad (6)$$

164 We assume that increased *ISR* (workload in the sense of [26]) leads to an increase in σ whereaσ increaσed
165 M leads to a decrease in σ.

166 The slowest and final form of compensation for insulin resistance is increased beta-cell mass, β, which
167 develops over years in humans. We assume that β is increased by proliferation, P, and decreased by
168 apoptosis, A. Following the data of [26], we assume that P increases when *ISR* increases. We further
169 assume that apoptosis is largely driven by metabolic stress (e.g. through increased production of reactive
170 oxygen species) when glucose is high, so we make A an increasing function of M :

171 $$\frac{d\beta}{dt} = \frac{(P(ISR)-A(M))\beta}{\tau_\beta} \quad (7)$$

172

The parameters defining P and A are chosen such that modest increases in G result in a net increase in β, but large increases in G result in a net decrease in β. As in the predecessor model of [7], this leads to a shift from compensation (negative feedback) to decompensation (positive feedback). In [6], we showed that this can account for the threshold behavior observed in both rodents and humans, that is, nearly steady G followed by a sharp, essentially irreversible increase [27,28]. We proposed this as an explanation for why prevention of T2D is much easier than reversing it once it is established. The same dynamic properties carry over in this study with the model enhanced as described next.

New features in the model

Modeling glucose flux during daily meals and glucose tolerance tests

In the previous version of the model [6], G represented average daily glucose and insulin levels in response to steady glucose input. To address IFG and IGT, we need to be able to dissociate fasting glucose from post-challenge glucose. The first step is to introduce variable glucose influx from meals, represented by the term *MEAL* in Eq. (1). Timing of meals is standardized to 6:00 AM, 12:00 Noon, and 6:00 PM. The expression is given in Eq. (A1), and Fig. A3 shows the glucose flux (panel A) and the resulting plasma glucose concentrations (panel B). We do not yet account for other nutrients (amino acids, fats). Flux during an OGTT is modeled with a more rapid rise and decay of flux (Eq. (A2) and shown in Fig. A3, C, D). Flux during an IVGTT rises and decays still more rapidly.

Modeling hepatic glucose production (HGP)

In order to distinguish peripheral and hepatic insulin resistance and describe how they are related to each other, we need to refine the model description of hepatic glucose production (*HGP* in Eq. 1). In the first

195 version of the model [6], *HGP* was assumed to be constant, which is an acceptable approximation as long as
196 fasting plasma insulin is adequate to compensate perfectly for any hepatic insulin resistance. To study the
197 failure of compensation, however, we need to make *HGP* dependent on *I* (Eq. A4). This is sufficient to
198 give the typical drop and recovery of *HGP* after a meal (Fig. A4, A). Figure A6, E – H shows the
199 response of HGP and glucose disposal to a simulated hyperinsulinemic, euglycemic clamp, with steady-
200 state values in good agreement with experimental data [29].

201 Less obvious, but also important, we need to account for the correlation between hepatic and peripheral
202 insulin resistance, which we do by making two of the parameters in Eq. A4, $hepa_{max}$ and $\alpha_{HGP,}$ functions
203 of S_I (Eqs. A5, A6 and Fig. A4, B, C). If this is not done, then in a case of severe peripheral resistance
204 with strong compensatory insulin secretion, it is possible to have fasting hypoglycemia, which is not the
205 typical pattern (See Fig. A7). In more typical cases of progression to pre-diabetes or diabetes, the
206 relative impairment in insulin secretion would mask this effect: the level of glycemia would be reduced
207 but hypoglycemia would not result. We choose the parameters such that HGP remains normal when
208 insulin is elevated unless there is a defect in beta-cell mass or function. To represent hepatic insulin
209 resistance over and above the component related to peripheral insulin resistance, we decrease the
210 parameter $hepa_{SI}$ in Eq. A4, which increases HGP at any value of *I*.

211

212 *Modeling insulin granule exocytosis*

213 To study the dynamics of glucose and insulin under glucose challenges such as meals, OGTT, and
214 IVGTT, the model needs to account for the multiple kinetic components of insulin secretion. We adapted
215 an existing model of insulin granule exocytosis [18], which was designed to capture the biphasic pattern of
216 *ISR* in response to a glucose step in vitro or a hyperglycemic clamp in vivo. The first phase is
217 characterized by a sharp peak of *ISR* during the first 10 minutes and the second phase by a steady increase

of *ISR* over the next hour. Figure A6 shows a simulated OGTT (panels A, B) and a simulated IVGTT (panels, C, D) compared to experimental data.

These phases are mediated by progression of vesicles through a sequence of stages culminating in exocytosis (fusion with the plasma membrane and release of insulin to the circulation; Fig. A2A). A large reserve pool, treated as an inexhaustible reservoir, feeds the docked pool (vesicles at binding sites on the plasma membrane). Once docked, vesicles are primed and enter the readily releasable pool (RRP). Primed vesicles join the immediately releasable pool by becoming closely associated with voltage-dependent Ca^{2+} channels. First-phase secretion depends mainly on the size of the RRP at basal glucose, and second phase secretion is controlled by the rate of mobilization of vesicles to the docked pool.

The insulin secretion rate *ISR* in the first version [6] of the model (Eq. 3) is in the new version no longer a function of glucose, but is calculated as an output of the exocytosis model (Eqs. A11), *ISR* thus now depends on the history of exposure to *G*, as it should, not just the current value. The exocytosis model requires as input the cytosolic Ca^{2+} concentration, which is modeled as a sigmoidal function of the beta-cell metabolic rate *M* (Eq. A7), and the much higher Ca^{2+} concentration in the microdomains of Ca^{2+} channels, which is modeled as a function of cytosolic Ca^{2+} (Eq. A8). The dose response curve shift γ, previously included in Eq. 3, represents the dynamic changes in K(ATP) channel density as before, but now explicitly alters cytosolic Ca^{2+} at a given level of *M* (Eq. A7). Cytosolic calcium enhances the rates of mobilization of the reserve pool to the plasma membrane (Eq. A10) and priming of docked vesicles (r_2 in Eqs. A12), whereas vesicle fusion is primarily controlled by microdomain Ca^{2+}. The amplifying effect of glucose [21] is incorporated as a multiplicative factor in the rate of vesicle mobilization (G_F in Eq. A9). The effects of the incretins GLP-1 and GIP are effectively rolled into G_F but could be broken out as independent factors to study their dynamic changes over time or as targets of drug therapy, though we do not use that feature in this paper. For IVGTT and hyperglycemic clamp simulations, we reduce G_F by about a factor of two to represent the lack of the incretin effect on vesicle mobilization and reduce r_2^0 (Eq.

A12) about 10-fold to represent the lack of incretin effect on vesicle priming. The rate of mobilization (Eq. A11) is also assumed to be proportional to the variable σ (Eq. 6), which thus controls the magnitude of second-phase insulin secretion. As a consequence, *ISR* implicitly includes σ as a multiplicative factor, as in Eq. (3) of the simpler, first version of the model , and the dynamic evolution of the maximal secretory capacity over long time scales (months) is essentially equivalent.

Criteria of pre-diabetes and diabetes

Following the ADA criteria, we define IFG as FPG > 100 mg/dl but < 126 mg/dl, IGT as 2hPG > 140 mg/dl but < 200 mg/dl, and T2D as FPG ≥ 126 mg/dl or 2hPG ≥ 200 mg/dl. Combined glucose impairment (CGI) is defined as co-occurrence of IFG and IGT.

Software

The model equations are solved using xppaut [30] and Matlab (The Mathworks, Natick, MA). Input files defining the parameters and initial conditions are available on github at: https://github.com/artielbm/Pathways.

Results

In Figs. 1 – 4, we carry out longitudinal simulations over a period of five years starting in the NGT state in which either peripheral insulin resistance is dominant, in which case the first stage of hyperglycemia is IGT, or hepatic insulin resistance is dominant, in which case the first stage of hyperglycemia is IFG. These assumptions are applied by modeling peripheral and hepatic insulin sensitivity as exponentially

decreasing, using Eqs. A13 and A14, respectively. The initial values and rates of decline are the same for all figures, but the steady state (target) values, tar_{SI} and tar_{hepaSI}, are varied. The simulations calculate the daily responses to meals, but we plot only the results of OGTTs carried out periodically over the five-year time span by pausing the longitudinal simulation. The capacity of beta-cell function to compensate for insulin resistance is assumed to be limited, except in Fig. 2. The defect consists of a right shift in γ_∞ relative to Fig. 2, which can be interpreted as a slight gain of function mutation in KCNJ11, the Kir6.2 component of the KATP channels. Alterations in σ_∞ representing a mild defect in insulin granule mobilization would have a similar effect.

Parameters that were varied to make the figures are listed in Table S12A in the Appendix, and the initial conditions for Figs. 1 – 4 are in Table S12B.

IGT-first pathway

Figure 1 shows a longitudinal simulation of the effects of a strong decrease in peripheral insulin sensitivity S_I (Fig. 1A) combined with a mild decrease in hepatic insulin sensitivity, $hepa_{SI}$ (Fig. 1B). As insulin resistance progresses, 2hPG increases rapidly while FPG increases more slowly (Fig. 1C), resulting in progression from normal glucose tolerance (NGT) to IGT, CGI and ultimately T2D (Fig. 1C).

Fasting plasma insulin (FPI) and 2-hour plasma insulin (2hPI) rise as the beta cells initially compensate partially for the insulin resistance, then fall as the beta cells fail (Fig. 1D), following the classic "Starling law" of the pancreas [31]. The initial rise in secretion results from an increase in beta-cell sensitivity to glucose (the variable γ increases, not shown), and the decline results from a fall in the slower component of beta-cell function, σ (Fig. 1E). Beta-cell mass (β) also rises and falls, but the variation is limited because of the slowness of β, and the fall occurs only after T2D is already underway (Fig. 1F). This

accords with observations that beta-cell mass is elevated in insulin-resistant pre-diabetics but reduced in long-standing diabetes [32,33].

A subtle but important point of this simulation is that insulin resistance in both the liver and peripheral tissues reaches saturation (Fig. 1A, B) well before the advent of T2D. It is rather the continuing fall in beta-cell function, σ, that drives conversion to T2D. The same sequence was seen in the simulation of T2D progression in Zucker diabetic fatty rats (Fig. 6 in [6]) and in data from monkeys [34].

The fall in σ is triggered by the hyperglycemia and glucotoxicity that follows the early loss of insulin sensitivity (Fig. 1D) but would not lead to T2D if the pre-existing capacity of beta-cell function to compensate were stronger. This is illustrated by a simulation with the same degree of insulin resistance as in Fig. 1, but a milder beta-cell defect, which mimics a non-diabetic subject with insulin resistance (Fig. 2). FPG and 2hPG increase modestly in response to insulin resistance and reach a plateau in the IGT state as σ levels off (Fig. 2E) and plasma insulin plateaus (Fig. 2D). The limitation of the rise in glucose reduces the effects of glucotoxicity and buys time for beta-cell mass to increase and stabilize the IGT state (Fig. 2F).

Figures 1 and 2 together paint a picture in which not only is a combination of insulin resistance and impaired secretion necessary for T2D, but insulin resistance develops and saturates first, and T2D develops only if the beta cells fail. Some defect in beta-cell function is required even for pre-diabetes, in agreement with [35]. Conversely, a pre-existing defect in insulin secretion would be silent in the absence of insulin resistance (not shown).

IFG-first pathway

In Fig. 3 we illustrate a contrasting case to Fig. 1, dominant hepatic insulin resistance with minor peripheral resistance (Fig. 3A, B); the same beta-cell function defect is assumed as in Fig. 1. Hepatic insulin resistance drives FPG across the threshold for IFG, while 2hPG remains below the threshold for IGT (Fig. 3C). After the initial threshold crossing, however, FPG and 2hPG continue to rise, and IFG progresses to CGI as in Fig. 1. Insulin again rises with the help of γ (not shown) and falls when the drop in σ becomes too great (Fig. 3E). As in the IGT-first pathway, the conversion to T2D is driven mainly by reduced beta-cell function, σ, because insulin resistance in both the liver and peripheral tissues saturates well before T2D (or even CGI) begins. Beta-cell mass again plays a minor role (Fig. 3F).

In the BLSA some subjects who had progressed from NGT to IGT went on to T2D at the next follow-up, which prompted the authors to ask whether CGI could be skipped [2]. Figure 4 demonstrates that this can happen if peripheral insulin resistance is made much greater than hepatic resistance (compare Fig. 4A to Fig. 1A). Extreme loss of peripheral insulin sensitivity causes 2hPG to rise dramatically, while FPG remains in the normal range, converting NGT to IGT. 2hPG continues to deteriorate without a substantial increase in FPG, resulting in progression of IGT to T2D without passing through CGI. Eventually, FPG crosses the thresholds for IFG and T2D, but after the individual has already reached T2D based on 2hPG.

Figures 1 and 3, respectively, consider extreme cases of peripheral insulin resistance (PIR), where S_I dominates, and hepatic insulin resistance (HIR), where $hepa_{SI}$ dominates . However, most people on the path to T2D will have both. A composite view of the cases of Figs. 1 and 3 together with intermediate phenotypes is given in Fig. 5, where trajectories are plotted in the FPG – 2hPG plane. The only difference among the trajectories is the degree of HIR and PIR, varied inversely from lower right to upper left; the compensatory capacity of beta-cell function is identical for all traces. Fig. 5A shows that the trajectories diverge markedly as the defects in HIR and PIR set in but converge as hyperglycemia worsens; this happens because IFG induces IGT and IGT induces IFG. Thus, all the virtual patients end up looking the same as time goes on. The latter part of the NGT stage and the early part of the IGT stage,

shown expanded in Fig. 5B, are when the underlying pathologies give rise to the most distinct behavior. This is important both for designing clinical studies and for stratifying patients for treatment. The figure suggests that the slope of the trajectory from two or more OGTTs spaced suitably far apart in time could give a good indication of the future path of the patient.

We next look more closely at the pathogenesis process as it would appear clinically by simulating OGTTs (Fig. 6) and IVGTTs (Fig. 7) at representative times for each stage of glucose tolerance, indicated by the black circles on the time axes in Figs. 1C and 3C.

Simulation of OGTTs

Figure 6A, C shows representative glucose and insulin profiles during OGTTs at each stage of the IGT-first pathway of Fig. 1. Insulin concentrations at the IGT stage (Fig. 6C, dotted curve) are increased compared to NGT (Fig. 6C, solid curve) but are inadequate to maintain normoglycemia at two-hours because of the decreased peripheral insulin sensitivity (Fig. 1A). In contrast, the level of fasting insulin at IGT (Fig. 6C, dotted curve) is sufficient to maintain fasting glucose within the normal range because hepatic insulin resistance is relatively mild (Fig. 1B). During CGI, glucose (Fig. 6A, dashed curve) is increased at all time points compared to IGT, while the insulin level (Fig. 6C, dashed curve) is slightly diminished at the early time points (relative to glucose, however, secretion is impaired at all time points). This indicates that even progression to CGI from IGT is mainly due to impaired beta-cell function. Further and more marked decreases in insulin, due to impaired secretion at all time points during the OGTT, lead to diabetes (dot-dashed curve). Thus, during the progression towards T2D, insulin at all time points during the OGTT first increases and then decreases, in accord with the Starling Law [31].

Figure 6B, D shows glucose and insulin at each stage of the IFG-first pathway of Fig. 3. Severe hepatic insulin resistance increases glucose at all time points during the OGTT (Fig. 6B). The increase in FPG is

greater than for 2hPG, so the threshold for IFG is crossed first in Fig. 3. Even though fasting insulin at the IFG stage (Fig. 6D, dotted curve) is very high, it is not enough to maintain normal FPG, because of the severe hepatic insulin resistance (Fig. 3B). However, 2hPG is maintained in the normal range because peripheral insulin resistance is mild (Fig. 3A). Since both peripheral and hepatic insulin sensitivity saturate before the onset of CGI (Fig. 3A, B), the decrease in insulin at all time points during the OGTT (Fig. 6D, dashed curve) due to falling beta-cell function (Fig. 3E) is the main contributor to the progression to CGI from IFG and then to T2D.

Simulation of IVGTTs

Figures 1 – 6 highlight the importance of secretion defects, in the context of insulin resistance, in all the pathways to T2D, but now we break out the contributions of early vs. late secretion. First-phase secretion is widely considered a key early marker of future progress. For example, the classic paper [36] reported a cross-sectional study of IVGTTs, and showed that AIRg declines as FPG rises and is nearly gone by the time FPG reaches 115 mg/dl, well below the threshold for T2D. This supports the use of AIRg, and by implication first-phase insulin secretion, as an early marker for T2D. We now show that the model can reproduce the negative correlation between FPG and AIRg, but that rising FPG is not necessarily the sole or proximal cause of the decline in AIRg.

Figures 7A, B show simulations of the insulin responses during IVGTTs performed during the IGT-first and IFG-first pathways, respectively. AIRg is blunted and then vanishes in both pathways as FPG rises, as found in [36], but 2hPG also rises at the same time, albeit to different degrees relative to FPG in the two pathways. The decline of AIRg is more rapid than seen experimentally along both pathways [37], but the main point is that it results from the decline of RRP size (Figs. 7C, D), which is more fundamental than the level of glycemia, as the next two paragraphs explain.

RRP size is controlled by two factors, the rate of secretion, which determines the rate of vesicle efflux from the RRP and the rate of vesicle influx into the RRP from the docked pool. High FPG increases the rate of efflux in the basal state, so the RRP will already be depleted when the IVGTT commences, and AIRg will consequently be reduced. The rate of influx depends on the size of the docked pool and the rate of priming of docked vesicles. The rate of priming does not vary much in our simulations, but the size of the docked pool does, depending mainly on the rate of docking, which is proportional to one of our beta-cell function variables, σ. Although modest increases in glucose stimulate vesicle docking, larger increases cause glucose toxicity, which reduces σ and hence docking.

Because σ is slow, it responds to the average daily glucose, including the contributions of both fasting and post-prandial glucose, which differ according to pathway. Along the IGT-first pathway (Figs. 1 and 7A, C), AIRg initially declines primarily because of reduced σ (Fig. 1E), which is mainly determined by high post-prandial glucose, rather than FPG. Positive feedback in turn drives post-prandial glucose higher as σ decreases (Figs. 1C, E). Thus, the loss of AIRg and first-phase secretion is an indirect consequence of diminished second-phase secretion capacity. As the subject progresses to CGI, FPG also rises and further reduces AIRg due to pool depletion. In contrast, during the IFG-first pathway (Figs. 3 and 7B, D), the early rise of FPG reduces AIRg by depleting the RRP, and positive feedback from the later rise of 2hPG further diminishes AIRg by driving down σ.

In summary, reduced AIRg can be a marker of impairment in either first- or second-phase secretion, and, as glycemia progresses towards T2D, is likely to indicate both.

Targeted Drug Therapy

With the previous, simpler model [6] we showed that NGT and T2D were bistable states separated by a threshold. This accounted for the well-known observation that it is easier to prevent T2D than to reverse

it. The new model retains these characteristics but raises the possibility that the response to therapeutic interventions may vary depending on which pathway a patient follows to T2D. Figure 8 shows that this is indeed the case, and that knowledge of a patient's subtype of insulin resistance can in principle lead to more effective drug therapy.

Figures 8A, B contrast two drug therapies targeted to peripheral vs. hepatic insulin resistance in patients in the early stages of diabetes. Figure 8A shows glucose for a patient on the IGT-first pathway with dominant peripheral insulin resistance as in Fig. 1, in the absence of therapy (control, black curves) or in response to a high dose of a drug targeted to peripheral insulin resistance (dashed curves) or a drug targeted to hepatic insulin resistance (dotted). The high dose of the appropriately targeted drug only transiently improves FPG and 2hPG and ultimately fails to reverse T2D. Nonetheless, it is more effective at delaying progression than the mistargeted drug.

Figure 8B represents the complementary case, a patient on the IFG-first pathway with dominant hepatic insulin resistance, as in Fig. 3. The same treatments are applied, and, as in panel A, both drugs only transiently improve FPG and 2hPG, but the appropriately targeted drug is more effective at delaying progression.

Figures 8C, D show the same drug therapies and progression pathways as in panels A and B, but with the drugs applied before the onset of diabetes. A low dose of a drug targeted to the patient's specific insulin resistance pathology is in both cases now able to prevent progression to diabetes, while a low dose of a mistargeted drug only delays progression. These examples suggest that the effectiveness of drug therapy depends on both early initiation of treatment and detection of the major metabolic abnormality.

The study in [13] found that it was necessary to assume that the efficacy of treatment wanes with time in order to fit the data from lifestyle and drug interventions in the DPP. Here we have shown that even if the

efficacy of treatment is maintained, the intrinsic dynamics of progressive beta-cell dysfunction can cause treatment to fail.

Caution should be used in interpreting the simulated treatments in Fig. 8 in terms of currently used drugs. For example, in the DREAM study [38] it was found that rosiglitazone was effective in cases of isolated IFG (IIFG), that is IFG in the absence of IGT. Although rosiglitazone is often thought of as primarily improving peripheral insulin sensitivity, it also improves hepatic insulin sensitivity [39]. In addition, IIFG does not necessarily imply pure hepatic insulin resistance. For example, a person with FPG = 115 and 2hPG = 135 would be classified as IIFG but may have significant peripheral insulin resistance. Most individuals with pre-diabetes likely have a mixture of peripheral and hepatic insulin resistance.

Discussion

In recognition of the fundamental character of type 2 diabetes (T2D) as a progressive disease that develops over many years, we have established a longitudinal model for its pathogenesis. We follow in the footsteps of other longitudinal models [7,10,13] but offer new clinical applications and insights.

We apply the model to analyze the diverse presentation of hyperglycemia, which may manifest first in fasting glucose (IFG-first pathway) or two-hour glucose during an OGTT (IGT-first pathway). To carry out this program, we modified the representation for beta-cell response to insulin resistance in the model of [6], enhancing it to differentiate between hepatic and peripheral insulin resistance. The simulations show that heterogeneity in the degree of the two forms of insulin resistance can account for a wide variety of observed patterns, supporting the idea of T2D as a unitary disease with quantitative variants. We have focused on extreme cases to highlight the differences (e.g. Fig. 1 vs. Fig. 3), but the family of trajectories in the FPG-2hPG plane (Fig. 5) shows that these lie on a continuum. Figure 5 also highlights that

differences in insulin resistance phenotype are most evident in the late NGT and early pre-diabetes stages, which are thus most amenable to differential phenotyping and therapeutic stratification.

We have incorporated a description of insulin granule dynamics sufficient to account for both first- and second-phase insulin secretion. This made it possible to simulate OGTT and IVGTT time courses and show how they are transformed systematically during progression along the two canonical pathways to diabetes (Figs. 6, 7). We also showed that sufficiently strong beta-cell function can prevent T2D even when insulin resistance is severe, allowing individuals to maintain a permanent state of IGT (Fig. 2) or even revert from IGT to NGT (not shown). Conversely, sufficient insulin sensitivity can prevent T2D even when beta-cell function is somewhat impaired [6]. As discussed below, a fuller treatment of the differences in the balance of insulin secretion and insulin action defects is needed to account fully for the diverse patterns of T2D progression.

We summarize below the specific lessons learned and questions answered by this study and give a preview of the clinical applications we anticipate for the model.

Questions raised in the BLSA and other studies

The BLSA study [2] asked whether subjects who enter the IGT state necessarily pass through CGI on the way to T2D. The model suggests (Fig. 4) that this is not the case, but skipping CGI happens only if the peripheral insulin resistance is markedly greater than hepatic insulin resistance, so this is expected to occur only rarely. An intermediate possibility predicted by the model is a short, but not absent, interval of CGI that could escape detection if the follow-up interval is too long.

A parallel question is whether individuals can go directly from IFG to T2D without passing through CGI. This is harder than going directly from IGT to T2D because 2hPG is much more labile than FPG; it is difficult to get an increase in FPG sufficient to cross the threshold for T2D (125 mg/dl) without at the

same time having 2hPG cross the threshold for IGT (140 mg/dl). Indeed, we have not been able to simulate this scenario just by choosing an appropriate mixture of hepatic and peripheral insulin sensitivity using the other parameters as in Figs. 1 – 4, but model simulations (not shown) predict that it can happen if a more severe beta-cell defect (in γ_∞, Eq. A15) is assumed.

The BLSA study also asked whether individuals can pass directly from NGT to T2D without passing through any pre-diabetic state. Because glucose is in quasi-steady state with the much slower variables representing beta-cell mass, beta-cell function and insulin sensitivity, this is not possible in the model unless one of those slow variables undergoes a catastrophic, virtually discontinuous, change. Pancreatectomy would be an example of this, but even type 1 diabetes, triggered by a rapid fall in beta-cell mass, has a distinct prediabetes phase. The cases observed in BLSA in which subjects were NGT at baseline and T2D at first follow-up most likely reflected rapid progression or a long gap between visits. Similarly, the model simulations indicate that it is unlikely for individuals to go from NGT to CGI without passing through IFG or IGT.

The BLSA reported that IFG is generally followed by IGT and IGT is generally followed by IFG, and the model suggests that each state *induces* the other. This happens because the initial rise in glucose during IFG impairs beta-cell function, which causes 2hPG to rise, and vice versa. Another study raised the question of whether CGI is a progressed state of IFG [40]; the model simulations together with the BLSA data show that CGI may instead be a progressed state of IGT, to which IFG has been added.

One can also ask whether crossing the threshold for FPG or 2hPG of pre-diabetes predicts whether T2D will be reached by crossing the corresponding threshold. In Fig. 1, IGT is followed by T2D diagnosed through 2hPG, and further simulations with the model (Fig. 5) suggest that this is typical. In Fig. 3, IFG is followed by T2D diagnosed through FPG, but further simulations (not shown) indicate that this may or may not be the case, depending on the degree of discrepancy between HIR and PIR and the strength of γ to control FPG.

494 Both the IFG- and IGT-first pathways exhibit elevated fasting insulin. This may account for the
495 observation that elevated fasting insulin was a better predictor of future diabetes in a prospective study
496 than fasting glucose, which is only elevated early on in the IFG-first pathway [41]; it may not be necessary
497 to hypothesize a major causative role for high fasting insulin itself. Indeed, in the IGT-first pathway,
498 which is more common, fasting glucose may be suppressed by the compensatory increase in beta-cell
499 function (our variable σ) induced by high post-load glucose (compare Figs. 1 and 4 to Fig. 3).

500 The suppression of fasting glucose in the context of a predominance of peripheral insulin resistance has
501 particular importance for pre-diabetes screening in populations that are prone to IGT but not IFG. This
502 applies notably to people of African descent, for whom fasting glucose has markedly reduced sensitivity
503 for detecting pre-diabetes and diabetes [42]. The problem is exacerbated for Africans living in Africa,
504 where measuring 2hPG with OGTTs is prohibitively expensive. The model suggests that in this and
505 similar cases, lowering the threshold for diagnosing pre-diabetes based on fasting glucose could be a cost-
506 effective strategy. More generally, the model points to the need for population- and patient-specific
507 thresholds for diagnosis, which may contribute to resolving current debate on whether prediabetes is a
508 useful diagnosis [43].

509

510 ***Peripheral and hepatic insulin resistance are not independent***

511 We have varied peripheral and hepatic insulin resistance independently to study their contributions to
512 T2D progression, but in reality, they are related. Statistically, they are correlated with a coefficient of
513 about 0.7 [44]. This is expected for several reasons. For one, they share major components of the insulin
514 signaling pathway. Also, there is evidence that an important determinant of hepatic insulin resistance is
515 excess supply of free fatty acid (FFA) substrate from adipose tissue [45]. Thus, insulin resistance in
516 adipose cells would increase lipolysis and FFA flux to the liver, which would drive increased

gluconeogenesis [46]. On the other hand, the liver has unique roles in glucose and lipid production not shared with muscle, which may account for the fact that the correlation is imperfect.

The unique contribution of the model in this regard, however, is to reveal *dynamic* reasons for a relationship between hepatic and peripheral resistance. Fasting HGP is primarily controlled by fasting insulin concentration, but post-prandial HGP is suppressed by the post-prandial rise of insulin. If severe peripheral insulin resistance is present, but the compensation in insulin is strong, it is possible to have fasting hypoglycemia unless there is some degree of hepatic insulin resistance. This is illustrated in Fig. A7. Since this is not typically observed, we have accounted for this by making HGP dependent on S_I (Eqs. A4 - A6, Fig. A4), reflecting the above-mentioned correlation between hepatic and peripheral resistance. Note that we have omitted glucagon from the model for simplicity because we are not aware of strong evidence that it is involved in the development of diabetes, though it is involved in worsening hyperglycemia in established diabetes. It is possible that glucose may also contribute to avoiding hypoglycemia under the conditions of severe insulin resistance and strong secretion described in this paragraph.

To address hepatic insulin resistance above and beyond the component correlated with peripheral insulin resistance, we have independently varied the affinity of HGP for insulin (parameter $hepa_{SI}$ in Eq. A4), the effect of which is shown in Fig. A4. We have obtained similar results (not shown) by varying the maximal rate of HGP (parameter $hepa_{max}$).

Secretion defects

The simulations of progression to T2D (Figs. 1, 3, and 4) require some degree of secretion defect in addition to the various combinations of insulin resistance. We assumed a defect only in the triggering pathway (γ), but we have obtained similar results by assuming defects in the amplifying pathway (σ).

The assumed triggering defect represents a right shift in the glucose dose response curve, which corresponds to a mild gain of function mutation of the K(ATP) channels, a prominent hit in GWAS [47].

The model shows that defects in first- and second-phase secretion are not independent. Impairment in one leads to impairment in the other because of the harmful effects of elevated glucose. The model accounts for classic data [36] showing that the acute insulin response to glucose (AIRg), a surrogate for first phase secretion, declines with even modest increases in FPG during the NGT and pre-diabetic stages. The model shows, however, that second-phase insulin secretion declines in parallel, belying a privileged role for first-phase secretion, as also shown in another modeling study [48]. In our model, reduced AIRg results mainly from reduced size of the RRP, which can be caused by impairment in either first-phase or second-phase secretion or both. More generally, any unanswered rise in either fasting or post-prandial glucose impairs both first and second phase secretion, and any defect in either first or second phase secretion raises both fasting and post-prandial glucose. This creates a vicious cycle that drives down both first- and second-phase secretion regardless of which defect is primary. Empirical studies that do not select for early isolated FPG or IGT cases do not show a clear prominence of first phase secretion loss [49], in agreement with the model.

Limitations of the study

For simplicity and brevity, we addressed here only the contributions of hepatic and peripheral insulin resistance in driving the IFG-first and IGT-first pathways. It has been shown, however, that non-insulin-dependent glucose uptake (glucose effectiveness) also plays a role [40]. The model can account for this if the glucose effectiveness parameter E_{G0} in Eq. (1) is varied. We have also found that a right shift in the sensitivity of the beta cells to glucose (our function $\gamma_\infty(G)$ in Eqs. (5, A15)) can by itself or in combination with hepatic insulin resistance cause IFG and alter the trajectory of IGT.

563 The model as presented here is also oversimplified in that it only considers glucotoxicity and neglects
564 other factors that are likely to play a role, such as lipotoxicity [50]. In addition, we believe that prolonged
565 high secretion rate is probably harmful beyond the negative effect incorporated in the equation for σ,
566 possibly because of ER stress and/or calcium toxicity [51]. Those factors were not included here because
567 they were not needed to account for the pathways considered, but they may be necessary to explain other
568 pathways to T2D and will be addressed elsewhere.

569 To capture the full range of patterns, it is necessary to consider as well pre-existing variation in beta-cell
570 function, not the moment-to-moment beta-cell function, which evolves in response to hyperglycemia, but
571 the innate, genetic capacity of beta-cell function to adapt to hyperglycemia. For example, changing the
572 parameters defining σ_∞ (Eqs. 6, A16) has marked effects on the speed of progression in IGT; we
573 neglected this because it doesn't change the likelihood of entering the IGT state much.

574 We have modeled the suppression of hepatic glucose production as a direct effect of insulin on the liver.
575 However, much if not all of the acute effect of insulin is indirect, mediated by suppression of lipolysis in
576 adipose tissue, which reduces the supply of free fatty acid (FFA) to the liver [45]. We consider this an
577 acceptable approximation for our purposes, as post-prandial suppression of lipolysis is roughly a mirror
578 image of the post-prandial rise in insulin. In future, if we want to account for FFA dynamics or adipose-
579 tissue insulin resistance, the model would have to be augmented.

580 We have modeled insulin-dependent glucose uptake as linear in insulin, but it is likely to be non-linear
581 (sigmoidal) [52] and has been suggested to exhibit hysteresis [53]. We have not found these features to be
582 necessary to explain the data under consideration, but they can be easily added in the future if the need
583 arises.

584 We have included only a very simple representation of insulin clearance, assuming a first-order
585 dependence on insulin concentration. We have not distinguished portal from peripheral insulin [54] or
586 considered possible regulation by glucose [55] or free fatty acids [56].

587 A question of particular current interest with regard to clearance that we have not investigated here is
588 what contribution clearance makes to the pathogenesis of T2D. There is considerable evidence that
589 insulin clearance is positively correlated with peripheral insulin sensitivity (e.g., [54,57]), but the direction of
590 causation is not clear. If clearance is reduced secondary to reduced overall insulin sensitivity, then it
591 would contribute to the compensatory response, along with increased insulin secretion. However, it has
592 been suggested that the increased insulin resulting from reduced clearance may also contribute to insulin
593 resistance [58]. If that effect is modest in magnitude, it may reduce or even eliminate the compensatory
594 contribution of reduced clearance.

595 If the effect of hyperinsulinemia is great, or is even the primary cause of insulin resistance, as suggested
596 in [57], it could possibly itself drive the pathogenesis of diabetes. Along those lines, it has been shown that
597 knocking out a key enzyme regulating insulin clearance, carcinoembryonic antigen-related cell adhesion
598 molecule 1 (CEACAM1), causes insulin resistance in mice [59]. The pathway involved is complicated,
599 involving direct effects on de novo lipogenesis in the liver and interactions with feeding circuits in the
600 hypothalamus in addition to hyperinsulinemia per se. It is beyond the scope of the present model but may
601 be an interesting topic for future modeling work.

602
603 ***Future directions***

604 This paper has demonstrated that if the insulin resistance phenotype of an individual is known, their
605 future trajectory of hyperglycemia can be predicted (Figs. 1 – 4) and drug choice can potentially be
606 optimized for the patient's insulin resistance phenotype (Fig. 8). Another longitudinal model has shown
607 similarly the results of targeting insulin resistance vs. beta-cell replication [9]. Our model can provide

similar predictions if the relative impairments in insulin secretion and insulin resistance are known. For example, plotting 1hPG vs. 2hPG obtained by simulating OGTTs results in a family of trajectories similar to the ones for FPG vs. 2hPG shown in Fig. 5. The differences in trajectories due to the contributions of insulin secretion and insulin action can be read off from the difference between 1hPG and 2hPG and are similarly most pronounced during prediabetes (Ha et al, ADA poster 1490-P, June, 2019). This prediction may provide deeper insight into the diagnostic information that can be extracted from different time points during the OGTT, an issue that is currently receiving much attention [19,60].

However, to be a useful tool for patient stratification and treatment planning, one needs to ascertain the patient's phenotype. We plan to investigate whether the model can be used, with suitable modifications, to solve the inverse problem of inferring the individual's parameters of insulin resistance and beta-cell function from the observed behavior.

Acknowledgments

The work was supported by the Intramural Research Program of the National Institutes of Health, NIDDK. We thank Stephanie Chung, Richard Bertram, Over Cabrera, and Cecilia Diniz Behn for helpful suggestions on the manuscript.

References

1. Knowler WC, Barrett-Connor E, Fowler SE, et al. Reduction in the incidence of type 2 diabetes with lifestyle intervention or metformin. *N Engl J Med*. 2002;346(6):393-403. doi:10.1056/NEJMoa012512

2. Meigs JB, Muller DC, Nathan DM, Blake DR, Andres R, Baltimore Longitudinal Study of Aging. The natural history of progression from normal glucose tolerance to type 2 diabetes in the Baltimore Longitudinal Study of Aging. *Diabetes*. 2003;52(6):1475-1484.

3. Kodama K, Tojjar D, Yamada S, Toda K, Patel CJ, Butte AJ. Ethnic differences in the relationship between insulin sensitivity and insulin response: a systematic review and meta-analysis. *Diabetes Care*. 2013;36(6):1789-1796. doi:10.2337/dc12-1235

4. Cobelli C, Dalla Man C, Toffolo G, Basu R, Vella A, Rizza R. The oral minimal model method. *Diabetes*. 2014;63(4):1203-1213. doi:10.2337/db13-1198

5. Mari A, Ferrannini E. Beta-cell function assessment from modelling of oral tests: an effective approach. *Diabetes Obes Metab*. 2008;10 Suppl 4:77-87. doi:10.1111/j.1463-1326.2008.00946.x

6. Ha J, Satin LS, Sherman AS. A Mathematical Model of the Pathogenesis, Prevention, and Reversal of Type 2 Diabetes. *Endocrinology*. 2016;157(2):624-635. doi:10.1210/en.2015-1564

7. Topp B, Promislow K, deVries G, Miura RM, Finegood DT. A model of beta-cell mass, insulin, and glucose kinetics: pathways to diabetes. *J Theor Biol*. 2000;206(4):605-619. doi:10.1006/jtbi.2000.2150

8. Karin O, Swisa A, Glaser B, Dor Y, Alon U. Dynamical compensation in physiological circuits. *Mol Syst Biol*. 2016;12(11):886.

9. Hardy T, Abu-Raddad E, Porksen N, De Gaetano A. Evaluation of a mathematical model of diabetes progression against observations in the Diabetes Prevention Program. *Am J Physiol Endocrinol Metab*. 2012;303(2):E200-212. doi:10.1152/ajpendo.00421.2011

10. De Gaetano A, Hardy T, Beck B, et al. Mathematical models of diabetes progression. *Am J Physiol Endocrinol Metab*. 2008;295(6):E1462-1479. doi:10.1152/ajpendo.90444.2008

11. Wang Y-F, Khan M, van den Berg HA. Interaction of fast and slow dynamics in endocrine control systems with an application to β-cell dynamics. *Math Biosci*. 2012;235(1):8-18. doi:10.1016/j.mbs.2011.10.003

12. Goel P. Insulin resistance or hypersecretion? The βIG picture revisited. *J Theor Biol*. 2015;384:131-139. doi:10.1016/j.jtbi.2015.07.033

13. De Gaetano A, Hardy TA. A novel fast-slow model of diabetes progression: Insights into mechanisms of response to the interventions in the Diabetes Prevention Program. *PLoS ONE*. 2019;14(10):e0222833. doi:10.1371/journal.pone.0222833

14. Choy S, Kjellsson MC, Karlsson MO, de Winter W. Weight-HbA1c-insulin-glucose model for describing disease progression of type 2 diabetes. *CPT Pharmacometrics Syst Pharmacol*. 2016;5(1):11-19. doi:10.1002/psp4.12051

15. de Winter W, DeJongh J, Post T, et al. A mechanism-based disease progression model for comparison of long-term effects of pioglitazone, metformin and gliclazide on disease processes underlying Type 2 Diabetes Mellitus. *J Pharmacokinet Pharmacodyn*. 2006;33(3):313-343. doi:10.1007/s10928-006-9008-2

16. Ribbing J, Hamrén B, Svensson MK, Karlsson MO. A model for glucose, insulin, and beta-cell dynamics in subjects with insulin resistance and patients with type 2 diabetes. *J Clin Pharmacol*. 2010;50(8):861-872. doi:10.1177/0091270009349711

17. Nyman E, Rozendaal YJW, Helmlinger G, et al. Requirements for multi-level systems pharmacology models to reach end-usage: the case of type 2 diabetes. *Interface Focus*. 2016;6(2):20150075. doi:10.1098/rsfs.2015.0075

18. Chen Y, Wang S, Sherman A. Identifying the targets of the amplifying pathway for insulin secretion in pancreatic beta-cells by kinetic modeling of granule exocytosis. *Biophys J*. 2008;95(5):2226-2241. doi:10.1529/biophysj.107.124990

19. Chung ST, Ha J, Onuzuruike AU, et al. Time to glucose peak during an oral glucose tolerance test identifies prediabetes risk. *Clin Endocrinol (Oxf)*. July 2017. doi:10.1111/cen.13416

20. Bergman RN, Ider YZ, Bowden CR, Cobelli C. Quantitative estimation of insulin sensitivity. *Am J Physiol*. 1979;236(6):E667-677.

21. Henquin JC. Triggering and amplifying pathways of regulation of insulin secretion by glucose. *Diabetes*. 2000;49(11):1751-1760.

22. Glynn E, Thompson B, Vadrevu S, et al. Chronic Glucose Exposure Systematically Shifts the Oscillatory Threshold of Mouse Islets: Experimental Evidence for an Early Intrinsic Mechanism of Compensation for Hyperglycemia. *Endocrinology*. 2016;157(2):611-623. doi:10.1210/en.2015-1563

23. Jones CN, Pei D, Staris P, Polonsky KS, Chen YD, Reaven GM. Alterations in the glucose-stimulated insulin secretory dose-response curve and in insulin clearance in nondiabetic insulin-resistant individuals. *J Clin Endocrinol Metab*. 1997;82(6):1834-1838. doi:10.1210/jcem.82.6.3979

24. Jung S-H, Jung C-H, Reaven GM, Kim SH. Adapting to insulin resistance in obesity: role of insulin secretion and clearance. *Diabetologia*. 2018;61(3):681-687. doi:10.1007/s00125-017-4511-0

25. Kim MK, Reaven GM, Kim SH. Dissecting the relationship between obesity and hyperinsulinemia: Role of insulin secretion and insulin clearance. *Obesity (Silver Spring)*. 2017;25(2):378-383. doi:10.1002/oby.21699

26. Porat S, Weinberg-Corem N, Tornovsky-Babaey S, et al. Control of pancreatic β cell regeneration by glucose metabolism. *Cell Metab*. 2011;13(4):440-449. doi:10.1016/j.cmet.2011.02.012

27. Mason CC, Hanson RL, Knowler WC. Progression to type 2 diabetes characterized by moderate then rapid glucose increases. *Diabetes*. 2007;56(8):2054-2061. doi:10.2337/db07-0053

28. Tabák AG, Jokela M, Akbaraly TN, Brunner EJ, Kivimäki M, Witte DR. Trajectories of glycaemia, insulin sensitivity, and insulin secretion before diagnosis of type 2 diabetes: an analysis from the Whitehall II study. *Lancet*. 2009;373(9682):2215-2221. doi:10.1016/S0140-6736(09)60619-X

29. Basu R, Barosa C, Jones J, et al. Pathogenesis of prediabetes: role of the liver in isolated fasting hyperglycemia and combined fasting and postprandial hyperglycemia. *J Clin Endocrinol Metab*. 2013;98(3):E409-417. doi:10.1210/jc.2012-3056

30. Bard Ermentrout. *Simulating, Analyzing, and Animating Dynamical Systems*. Philadelphia, PA: SIAM; 2002. http://www.math.pitt.edu/~bard/xpp/xpp.html.

31. DeFronzo RA. Lilly lecture 1987. The triumvirate: beta-cell, muscle, liver. A collusion responsible for NIDDM. *Diabetes*. 1988;37(6):667-687.

32. Rahier J, Guiot Y, Goebbels RM, Sempoux C, Henquin JC. Pancreatic beta-cell mass in European subjects with type 2 diabetes. *Diabetes Obes Metab*. 2008;10 Suppl 4:32-42. doi:10.1111/j.1463-1326.2008.00969.x

33. Saisho Y, Butler AE, Manesso E, Elashoff D, Rizza RA, Butler PC. β-cell mass and turnover in humans: effects of obesity and aging. *Diabetes Care*. 2013;36(1):111-117. doi:10.2337/dc12-0421

34. Bodkin NL, Metzger BL, Hansen BC. Hepatic glucose production and insulin sensitivity preceding diabetes in monkeys. *Am J Physiol*. 1989;256(5 Pt 1):E676-681.

35. DeFronzo RA, Tripathy D. Skeletal Muscle Insulin Resistance Is the Primary Defect in Type 2 Diabetes. *Diabetes Care*. 2009;32(Suppl 2):S157-S163. doi:10.2337/dc09-S302

36. Brunzell JD, Robertson RP, Lerner RL, et al. Relationships between fasting plasma glucose levels and insulin secretion during intravenous glucose tolerance tests. *J Clin Endocrinol Metab*. 1976;42(2):222-229. doi:10.1210/jcem-42-2-222

37. Brunzell JD, Robertson RP, Lerner RL, et al. Relationships between fasting plasma glucose levels and insulin secretion during intravenous glucose tolerance tests. *J Clin Endocrinol Metab*. 1976;42(2):222-229. doi:10.1210/jcem-42-2-222

38. DREAM (Diabetes REduction Assessment with ramipril and rosiglitazone Medication) Trial Investigators, Gerstein HC, Yusuf S, et al. Effect of rosiglitazone on the frequency of diabetes in patients with impaired glucose tolerance or impaired fasting glucose: a randomised controlled trial. *Lancet*. 2006;368(9541):1096-1105. doi:10.1016/S0140-6736(06)69420-8

39. Yki-Järvinen H. Thiazolidinediones and the liver in humans. *Curr Opin Lipidol*. 2009;20(6):477-483. doi:10.1097/MOL.0b013e3283321d37

40. Perreault L, Bergman BC, Playdon MC, Dalla Man C, Cobelli C, Eckel RH. Impaired fasting glucose with or without impaired glucose tolerance: progressive or parallel states of prediabetes? *Am J Physiol Endocrinol Metab*. 2008;295(2):E428-435. doi:10.1152/ajpendo.90354.2008

41. Dankner R, Chetrit A, Shanik MH, Raz I, Roth J. Basal-state hyperinsulinemia in healthy normoglycemic adults is predictive of type 2 diabetes over a 24-year follow-up: a preliminary report. *Diabetes Care*. 2009;32(8):1464-1466. doi:10.2337/dc09-0153

42. Utumatwishima JN, Chung ST, Bentley AR, Udahogora M, Sumner AE. Reversing the tide - diagnosis and prevention of T2DM in populations of African descent. *Nat Rev Endocrinol*. 2018;14(1):45-56. doi:10.1038/nrendo.2017.127

43. Piller C. Dubious diagnosis. *Science*. 2019;363(6431):1026-1031. doi:10.1126/science.363.6431.1026

44. Abdul-Ghani MA, Matsuda M, DeFronzo RA. Strong association between insulin resistance in liver and skeletal muscle in non-diabetic subjects. *Diabet Med*. 2008;25(11):1289-1294. doi:10.1111/j.1464-5491.2008.02597.x

45. Perry RJ, Camporez J-PG, Kursawe R, et al. Hepatic acetyl CoA links adipose tissue inflammation to hepatic insulin resistance and type 2 diabetes. *Cell*. 2015;160(4):745-758. doi:10.1016/j.cell.2015.01.012

46. Petersen MC, Shulman GI. Mechanisms of Insulin Action and Insulin Resistance. *Physiol Rev*. 2018;98(4):2133-2223. doi:10.1152/physrev.00063.2017

47. Odgerel Z, Lee HS, Erdenebileg N, et al. Genetic variants in potassium channels are associated with type 2 diabetes in a Mongolian population. *J Diabetes*. 2012;4(3):238-242. doi:10.1111/j.1753-0407.2011.00177.x

48. Grespan E, Giorgino T, Arslanian S, Natali A, Ferrannini E, Mari A. Defective Amplifying Pathway of β-cell Secretory Response to Glucose in Type 2 Diabetes: Integrated Modeling of in vitro and in vivo Evidence. *Diabetes*. December 2017. doi:10.2337/db17-1039

49. Gerich JE. Is reduced first-phase insulin release the earliest detectable abnormality in individuals destined to develop type 2 diabetes? *Diabetes*. 2002;51 Suppl 1:S117-121.

50. Lim EL, Hollingsworth KG, Aribisala BS, Chen MJ, Mathers JC, Taylor R. Reversal of type 2 diabetes: normalisation of beta cell function in association with decreased pancreas and liver triacylglycerol. *Diabetologia*. 2011;54(10):2506-2514. doi:10.1007/s00125-011-2204-7

51. Nichols CG, Remedi MS. The diabetic β-cell: hyperstimulated vs. hyperexcited. *Diabetes Obes Metab*. 2012;14(0 3):129-135. doi:10.1111/j.1463-1326.2012.01655.x

52. Bonadonna RC, Groop L, Kraemer N, Ferrannini E, Del Prato S, DeFronzo RA. Obesity and insulin resistance in humans: a dose-response study. *Metab Clin Exp*. 1990;39(5):452-459. doi:10.1016/0026-0495(90)90002-t

53. Wang G. Raison d'être of insulin resistance: the adjustable threshold hypothesis. *J R Soc Interface*. 2014;11(101):20140892. doi:10.1098/rsif.2014.0892

54. Polidori D, Bergman RN, Sumner AE. A New Model-Based Method for Estimating Hepatic and Peripheral Insulin Clearance from Intravenous Glucose Tolerance Test Data (2015 ADA abstract 254-LB).

55. Piccinini F, Dalla Man C, Vella A, Cobelli C. A Model for the Estimation of Hepatic Insulin Extraction After a Meal. *IEEE Transactions on Biomedical Engineering*. 2016;63(9):1925-1932. doi:10.1109/TBME.2015.2505507

56. Bergman RN, Ader M. Free fatty acids and pathogenesis of type 2 diabetes mellitus. *Trends Endocrinol Metab*. 2000;11(9):351-356.

57. Ader M, Stefanovski D, Kim SP, et al. Hepatic insulin clearance is the primary determinant of insulin sensitivity in the normal dog. *Obesity (Silver Spring)*. 2014;22(5):1238-1245. doi:10.1002/oby.20625

58. Piccinini F, Polidori DC, Gower BA, Bergman RN. Hepatic but Not Extrahepatic Insulin Clearance Is Lower in African American Than in European American Women. *Diabetes*. 2017;66(10):2564-2570. doi:10.2337/db17-0413

59. Ghadieh HE, Russo L, Muturi HT, et al. Hyperinsulinemia drives hepatic insulin resistance in male mice with liver-specific Ceacam1 deletion independently of lipolysis. *Metab Clin Exp*. 2019;93:33-43. doi:10.1016/j.metabol.2019.01.008

60. Hulman A, Witte DR, Vistisen D, et al. Pathophysiological Characteristics Underlying Different Glucose Response Curves: A Latent Class Trajectory Analysis From the Prospective EGIR-RISC Study. *Diabetes Care*. 2018;41(8):1740-1748. doi:10.2337/dc18-0279

61. DeFronzo RA, Tobin JD, Andres R. Glucose clamp technique: a method for quantifying insulin secretion and resistance. *Am J Physiol*. 1979;237(3):E214-223. doi:10.1152/ajpendo.1979.237.3.E214

62. Mari A, Pacini G, Murphy E, Ludvik B, Nolan JJ. A model-based method for assessing insulin sensitivity from the oral glucose tolerance test. *Diabetes Care*. 2001;24(3):539-548. doi:10.2337/diacare.24.3.539

63. Dalla Man C, Rizza RA, Cobelli C. Meal simulation model of the glucose-insulin system. *IEEE Trans Biomed Eng*. 2007;54(10):1740-1749. doi:10.1109/TBME.2007.893506

64. Muscelli E, Mari A, Natali A, et al. Impact of incretin hormones on beta-cell function in subjects with normal or impaired glucose tolerance. *Am J Physiol Endocrinol Metab*. 2006;291(6):E1144-1150. doi:10.1152/ajpendo.00571.2005

65. Mari A, Tura A, Pacini G, Kautzky-Willer A, Ferrannini E. Relationships between insulin secretion after intravenous and oral glucose administration in subjects with glucose tolerance ranging from normal to overt diabetes. *Diabet Med*. 2008;25(6):671-677. doi:10.1111/j.1464-5491.2008.02441.x

66. Rorsman P, Renström E. Insulin granule dynamics in pancreatic beta cells. *Diabetologia*. 2003;46(8):1029-1045. doi:10.1007/s00125-003-1153-1

67. Rorsman P, Braun M. Regulation of insulin secretion in human pancreatic islets. *Annu Rev Physiol*. 2013;75:155-179. doi:10.1146/annurev-physiol-030212-183754

68. Göpel S, Zhang Q, Eliasson L, et al. Capacitance measurements of exocytosis in mouse pancreatic alpha-, beta- and delta-cells within intact islets of Langerhans. *J Physiol (Lond)*. 2004;556(Pt 3):711-726. doi:10.1113/jphysiol.2003.059675

69. Breda E, Cavaghan MK, Toffolo G, Polonsky KS, Cobelli C. Oral glucose tolerance test minimal model indexes of beta-cell function and insulin sensitivity. *Diabetes*. 2001;50(1):150-158. doi:10.2337/diabetes.50.1.150

70. Chung ST, Galvan-De La Cruz M, Aldana PC, et al. Postprandial Insulin Response and Clearance Among Black and White Women: The Federal Women's Study. *J Clin Endocrinol Metab*. 2019;104(1):181-192. doi:10.1210/jc.2018-01032

Figure Legends

Figure 1: IGT-first pathway to diabetes. (A) Assumed severe decline in peripheral insulin sensitivity. (B) Assumed mild decline in hepatic insulin sensitivity. (C) Simulated longitudinal changes based on the assumptions in (A) and (B) in fasting plasma glucose (FPG) and two-hour glucose (2hPG) during OGTTs performed at each time point. The virtual subject experiences first high two-hour glucose (IGT), then high fasting glucose (CGI), and finally crosses the 2hPG threshold for T2D. (D) Simulated longitudinal changes in fasting plasma insulin (FPI) and two-hour insulin (2hPI) during the OGTTs. Insulin increases early on but decreases later. (E) The component of β-cell function represented by σ decreases progressively throughout. (F) The β-cell mass, β, first increases during prediabetes, then decreases after diabetes onset.

Figure 2: Insulin resistance (same as Fig. 1) does not lead to diabetes if beta-cell function is sufficiently responsive. The γ-dynamics is made stronger than in Fig. 1 by decreasing γ_s to 90 *mg/dl* from 100 *mg/dl* (see other parameters in Table S12A). (A) Assumed severe decline in peripheral insulin sensitivity. (B) Assumed mild decline in hepatic insulin sensitivity. (C) Simulated longitudinal changes in FPG and 2hPG during OGTTs performed at each time point. The virtual subject experiences modest rises in glucose and crosses the threshold for IGT but never crosses the thresholds for IFG, CGI or T2D. (D) Simulated longitudinal changes in fasting plasma insulin (FPI) and two-hour insulin (2hPI) during the OGTTs. Insulin concentration increases and saturates but never declines. (E) The β-cell function component σ first decreases, but then levels off. Increase in the β-cell function component represented by γ (not shown) helps limit the rise in glucose, which allows the β-cell mass β to increase gradually throughout (F).

Figure 3: IFG-first pathway to diabetes. (A) Assumed mild decline in peripheral insulin sensitivity. (B) Assumed severe decline in hepatic insulin sensitivity component $hepa_{SI}$. (C) Simulated longitudinal changes in FPG and 2hPG during OGTTs performed at each time point. The virtual subject experiences first high FPG (IFG), then high 2hPG (CGI), and finally crosses the FPG threshold for T2D first. Simulated longitudinal changes in fasting plasma insulin (FPI) and two-hour insulin (2hPI) during the OGTTs. Insulin concentration increases early on but decreases later. (E) The β-cell function component σ decreases progressively throughout. (F) The β-cell mass β increases during prediabetes then decreases after diabetes onset.

Figure 4: The CGI state is not obligatory. (A), (B): Extreme discrepancy between peripheral and hepatic (A – B) insulin resistance results in progression directly from IGT to T2D without passing through CGI based on OGTTs performed at each time point (C). FPG does not exceed the threshold for IFG until after T2D onset. (D) Simulated longitudinal changes in fasting plasma insulin (FPI) and two-hour insulin (2hPI) during the OGTTs. Insulin increases early on, then decreases. (E) The β-cell function component σ decreases more rapidly than in Figs. 1, 3. (F) The β-cell mass β increases during prediabetes, then decreases after diabetes onset.

Figure 5: (A) Two-hour glucose (2hPG) plotted vs. fasting glucose (FPG) for varying degrees of peripheral insulin sensitivity, S_I, and hepatic insulin sensitivity $hepa_{SI}$, starting from the same initial values as in Figs. 1 – 4 and evolving to the target values, tar_{SI} (Eq. A13) and tar_{hepaSI} (Eq. A14) as

follows: from upper left to lower right, the tar_{SI} values increase: 0.1, 0.17, 0.22, 0.33, 0.4 and 0.5; and the tar_{hepaSI} values decrease: 0.85, 0.6, 0.45, 0.35, 0.25 and 0.1. All other parameters are fixed. (B) expanded view of (A) to highlight the prediabetes region.

Figure 6: Glucose during OGTTs performed at the times indicated by the black dots in (A) Fig. 1 (IGT-first pathway) and (B) Fig. 3 (IFG-first pathway). (C, D) insulin corresponding to A and B, respectively. See text for details.

Figure 7: Insulin during IVGTTs performed at the time points indicated by the black dots in (A) Fig. 1 (IGT-first pathway) and (B) Fig. 3 (IFG-first pathway). (C, D): RRP size (numbers of vesicles) corresponding to A and B, respectively. Decline of AIRg parallels the reduction of RRP for each case.

Figure 8: Drug therapies targeting either peripheral insulin sensitivity (modeled as a rapid increase in S_I) or hepatic insulin sensitivity (modeled as a rapid increase in $hepa_{SI}$; see Tables S13 – S16 for details). The drugs are applied in the early stages of T2D (A, B) or during prediabetes (C, D). (A, C) Dominant peripheral insulin resistance, leading to IGT-first pathway as in Fig. 1. (B, D) Dominant hepatic insulin resistance, leading to IFG-first pathway as in Fig. 3. The appropriately targeted drug is more effective than the inappropriately targeted drug in each case, but therapy is more effective when initiated during prediabetes.

Appendix Figure Legends:

Fig. A1. Pathways to diabetes from the Baltimore Longitudinal Study of Aging. Data extracted from Fig. 3B of [2]. Of 362 subjects initially at NGT, 253 progressed to prediabetes (IFG, IGT or CGI) or T2D at first follow-up. A subset of each group had further follow-up, at which time some had progressed to T2D. In addition, some of the subjects who had initially progressed to IFG and IGT progressed further to CGI (Fig. 3A of [2]). Current ADA thresholds were used to define each category.

Fig. A2. A. Schematic of exocytosis model. Vesicles progress from the reserve pool to the docked pool, then the readily releasable pool (primed) and finally the immediately releasable pool (tethered to Ca^{2+} channels). B: Effect of high fasting glucose on first phase secretion rate. Control (solid): G sharply increased from 80 to 213 mg/dl with an exponential time course starting at time 0, matched to data from Fig. 1 in [61] (not shown). Parameters and variables as in Fig. 1, except the following variables, which are fixed: $\beta = 1000$, $\sigma = 1$; the G equation and its parameters are eliminated. Open circles: insulin response to the glucose from Fig. 1 in [61]. Dashed: Glucose raised to 213 mg/dl after equilibration at 110 mg/dl, reducing first-phase secretion. Parameters as for control, but σ reduced to 0.83 as expected for progression along IFG pathway. For both simulations, the implicit incretin effect is removed by reducing $G_{F_{max}}$C:10-fold and $r_2^0$14-fold. Effect of reduced σon second phase secretion. G is raised as in panel B, control, but with σ reduced 10% or 20% .

Fig. A3. Glucose fluxes and responses during meals and OGTTs. (A) Glucose flux in response to meals at 6:00 AM, 12:00 Noon, and 6:00 PM and (B) corresponding plasma glucose. Peak glucose flux during a meal of about 5 mg/dl/min, or 7.8 mg/kg/min, assuming 1.569 dL/kg [62], half-width of about 2 h and return to baseline in 7 h may be compared to Fig. 1 in [63]. (C) Glucose flux during an OGTT and (D) corresponding plasma glucose.

Fig. A4. Hepatic glucose production (HGP) as modeled by Eq. (A4). (A) HGP in response to a meal at time 0. (B) $hepa_{max}$, maximum of HGP given the level of insulin I, is modeled as a decreasing function of peripheral insulin sensitivity, S_I (Eq. A5). (C) α_{HGP}, representing the affinity of HGP for insulin, is modeled as a decreasing function of peripheral insulin sensitivity, S_I (Eq. A6). (D) Total HGP as a function of S_I , with I fixed at 30 μU/ml. Hepatic insulin sensitivity independent of peripheral insulin sensitivity is modeled by varying $hepa_{SI}$ in Figs. 1 - 7.

Fig. A5. Postprandial (PG) one hour after each breakfast, at 6:00 AM each day, and fasting (FG) glucose corresponding to Figs. 1, 2, 3, 4 is shown in A, B, C. and D, respectively. PG follows the same trends as two-hour glucose.

Fig. A6. Comparison of model simulations to selected experimental results. A, B: Glucose and insulin during an OGTT administered to a representative NGT person [64], Fig. 1 A, B: Parameters and variables are as in Fig. 1 except the following variables, which are fixed: $\beta = 1553$, $\sigma = 1$, $S_I = 0.5$ and $hepa_{SI} = 0.5$. C, D: Glucose and insulin during an IVGTT [65], Fig. 1C, D: Parameters and variables are as in Fig 1 except the following variables, which are fixed: $\beta = 1200$, $\sigma = 1$, $S_I = 0.8$ and $hepa_{SI} = 0.5$. E – H: simulation of a hyperinsulinemic, euglycemic clamp. Steady-state measured values from Fig. 2 in [29] are shown as grey ×'s. β and σ are set to 0 to reflect use of somatostatin to suppress endogenous insulin secretion. $S_I = 0.8$ and $hepa_{SI} = 1.0$, corresponding to an individual in the NGT range.

Fig. A7. A, C, E: Simulation of a case of very strong compensatory secretion, which preserves normal glucose tolerance in spite of a severe drop in S_I, from 0.8 to 0.2. The liver is insulin sensitive, with $hepa_{SI}$ maintained at 1.0, and beta-cell function is enhanced by increasing $\sigma_{ISR,max}$ to 2.1 (default=1.4). Hepatic glucose production (panel E) remains nearly constant because the effect of the drop in S_I on HGP balances the rise in fasting insulin. B, D, F: The same simulation but with S_I held fixed in Eqs. A5 and A6 at 0.8 while still declining in Eq. 1. Even though fasting insulin is lower in the right panels, the slight increase in fasting I over time causes HGP to decline, resulting in fasting hypoglycemia.

Appendix

Model equations repeated from main text

$$\frac{dG}{dt} = MEAL + HGP - (E_{GO} + S_I I)G$$

$$\frac{dI}{dt} = \frac{\beta}{V} ISR - kI$$

$$\frac{d\beta}{dt} = \frac{(P(ISR) - A(M))\beta}{\tau_\beta}$$

$$\frac{d\gamma}{dt} = \frac{\gamma_\infty(G) - \gamma}{\tau_\gamma}$$

$$\frac{d\sigma}{dt} = \frac{\sigma_\infty(ISR, M) - \sigma}{\tau_\sigma}$$

Where ~~t_{min}~~$=E_{G0}$ = 0.0118 min^{-1}, V = 7200 mL, and k = 0.446 min^{-1} (other parameters defined in tables below).

MEAL MODEL

$$MEAL = meal_{max}\left(\frac{t^{mk}}{\alpha_{meal}+t^{mk}}\right)^{\eta} \exp(-\mu t) \quad \text{(A1)}$$

Figs. A3 A, B show glucose fluxes and the corresponding glucose concentration in response to three meals per day.

Table S1. Parameters for *MEAL*

Parameter Name	Value	Description	Unit
$meal_{max}$	11.055	Maximum meal rate	*mg/dl/min*
mk	4	Degree of polynomial	unitless
α_{meal}	40	Half activation value	unitless

η	0.3	Exponent of rise for meal flux	unitless
μ	0.015	Rate of decay for meal flux	unitless

941

942

943 *OGTT MODEL*

944 Figs. A3 C, D show glucose fluxes and the corresponding glucose response during an OGTT. The OGTT
945 fluxes are modeled by a piecewise linear function similar to [4]. Specifically, the term *MEAL* in the *G*
946 equation is replaced by *OGTT*, where

947 $OGTT = \frac{OGTT_0}{V_G}$, where $V_G = BW \times \bar{V}$ is the volume of distribution for glucose in dL, BW is body weight
948 in kg, $\bar{V}$ = 1.569 dL/kg [62], and

949 $OGTT_0 = a_{i-1} + \frac{a_i - a_{i-1}}{t_i - t_{i-1}}(t - t_{i-1}), t_{i-1} < t < t_i, i = 1,2,3$ (A2)

950 $OGTT_o = 0$, elsewhere

951 The simulations in the paper were carried out assuming BW = 75kg, for a volume of distribution of 11.77
952 L, but this formulation makes the glucose load 75g independent of those choices. The values for a_i are
953 given in Table S2.

954

955 Table S2. Parameters for *OGTT*

Parameter name	Value	Description	Unit
a_0	0	Glucose flux at $t=t_0$	*mg/min*
a_1	588.5	Glucose flux at $t=t_1$	*mg/min*
a_2	353.1	Glucose flux at $t=t_2$	*mg/min*
a_3	0	Glucose flux at $t=t_3$	*mg/min*
t_0	0	Initial time of activation of glucose flux	*min*
t_1	15	First time of activation of glucose flux	*min*

t_2	120	Second time of activation of glucose flux	*min*
t_3	240	Third time of activation of glucose flux	*min*

IVGTT MODEL.

The rapid rise and decline in glucose flux are modeled by a polynomial and exponential function as shown in Figs. 6A, B, and C. The term *MEAL* in the *G* equation is replaced by *IVGTT*, where

$$IVGTT = \frac{IVGTT_{bar}}{BW\, V_G} t^{\kappa} \exp(-\lambda t) \quad \text{(A3)}$$

and $IVGTT_{bar}$ is given in Table S3 along with the other parameters. As for the OGTT, the simulations were carried out assuming $BW = 75$g.

Table S3 Parameters for *IVGTT*

Parameter name	Value	Description	Unit
$IVGTT_{bar}$	1.471×10^6	Maximum glucose flux	*mg/min*
κ	1	Degree of polynomial	unitless
λ	10	Decay rate of exponential function	1/min

Hepatic Glucose Production (HGP). HGP is modeled as a function of insulin concentration *I* and peripheral insulin sensitivity S_I using equations A4, A5, and A6. The model HGP is a decreasing function of *I* (Eq. A4): As *I* increases during the post-prandial state, HGP is suppressed (Fig. A4A). $hepa_{max}$ and α_{HGP} are modeled as decreasing functions of peripheral insulin sensitivity S_I, as shown in Figs. A4 B, C.

$$HGP = \frac{hepa_{max}}{\alpha_{HGP} + hepa_{SI}I} + HGP_{bas} \quad \text{(A4)}$$

$$hepa_{max} = \frac{hepa_{bar}}{hepa_k + S_I} + hepa_{sh} \quad \text{(A5)}$$

$$\alpha_{HGP} = \frac{\alpha_{bar}}{\alpha_k + S_I} + \alpha_{sh} \quad \text{(A6)}$$

974 Table. S4 Parameters for *HGP*

Parameter name	Value	Description	Unit
HGP_{bas}	0.104	Basal HGP rate	*mg/dl/min*
$hepa_{bar}$	15.443	Coefficient of $hepa_{max}$	10^{-4}*min(mg/dl/min)*
$hepa_{k}$	0.27	Translation of $hepa_{max}$	10^{-4}*ml/μU/min*
$hepa_{sh}$	-3.542	Shift of $hepa_{max}$	*(μU/ml)(mg/dl/min)*
α_{bar}	6	Coefficient of α_{HGP}	10^{-4}*/min*
α_{k}	0.4	Translation of α_{HGP}	10^{-4}*ml/μU/min*
α_{sh}	-0.5	Shift of α_{HGP}	*μU/ml*

975

976

977 *Bulk Cytosolic Calcium Concentration (C_i) Model.*

978 $$C_i = \frac{C_{i_{max}}(M+\gamma)^{kC_i}}{\alpha_{C_i}{}^{kC_i}+(M+\gamma)^{kC_i}} + C_{i_b} \qquad \text{(A7)}$$

979

980

981 Table S5 parameters for Ca^{2+} model

Parameter name	Value	Description	Unit
$C_{i,max}$	2	Maximum Ca^{2+}	*μM*
kC_i	4	Exponent of sigmoidal function	unitless
α_{Ci}	0.62	Half activation value	unitless
$C_{i,b}$	0.07	Basal calcium	*μM*

982

983

984 *Microdomain Ca^{2+} Concentration (C_{md}) Model*

985 $$C_{md} = \frac{C_{md_{max}}(C_i)^{kC_{md}}}{\alpha_{C_{md}}{}^{kC_{md}} + (C_i)^{kC_{md}}} + C_{md_b} \quad \text{(A8)}$$

986

987 Table S6 Parameters for Microdomain

988

Parameter name	Value	Description	Unit
$C_{md,max}$	150	Maximum C_{md}	μM
kC_{md}	4	Exponent of sigmoidal function	unitless
α_{Cmd}	1	Half activation value	unitless
$C_{md,b}$	0.0635	Basal microdomain calcium	μM

989

990

991 *Glucose Amplifying Factor Model.*

992 $$G_F = \frac{G_{F_{max}}(G - G_{F_{sh}})^{kG_F}}{\alpha_{G_F}{}^{kG_F} + (G - G_{F_{sh}})^{kG_F}} + G_{F_b} \quad \text{(A9)}$$

993

994 G_F implicitly includes a component corresponding to the incretin effect. For IVGTT and hyperglycemic
995 clamp simulations, we reduced $G_{F_{max}}$ by a factor of 10, which reduces G_F by a factor of about 2.

996

997 Table S7 Parameters for amplifying factor

Parameter name	Value	Description	Unit
$G_{F,max}$	4.45	Maximum value	unitless
$G_{F,sh}$	89	Shift of Glucose	*mg/dl*
kG_F	16	Exponent of sigmoidal function	unitless

$\alpha_{G,F}$	260	Half activation	*mg/dl*
$G_{F,b}$	1.78	Basal G_F	unitless

Insulin Granule Exocytosis Model. The model was previously published in [18]. The rate of mobilization of insulin granules, r_3, is modified to include a component of β-cell function, σ, and a glucose amplifying factor G_F that is modeled by a Hill function, whereas it was originally modeled by a step function in [18].

$$N_{1C} = \frac{km_1}{3k_1 C_{md} + rm_1}$$

$$N_{1D} = \frac{r_1}{3k_1 C_{md} + rm_1}$$

$$N_{2E} = \frac{3k_1 C_{md}}{2k_1\ C_{md} + km_1}$$

$$N_{2F} = \frac{2km_1}{2k_1\ C_{md} + km_1}$$

$$N_{3L} = \frac{2k_1 C_{md}}{2km_1\ +\ k_1 C_{md}}$$

$$N_{3N} = \frac{3km_1}{2km_1 + k_1 C_{md}} \qquad \text{(A10)}$$

$$C_{N4} = \frac{k_1 C_{md}}{2km_1\ +\ u_1}$$

$$C_{N3} = \frac{N_{3L}}{1 - N_{3N} C_{N4}}$$

$$C_{N2} = \frac{N_{2E}}{1 - N_{2F} C_{N3}}$$

$$C_{N1} = \frac{N_{1D}}{1 - N_{1C} C_{N2}}$$

$$\frac{dN_5}{dt} = t_s(rm_1 C_{N1} N_5 - (r_1 + rm_2) N_5 + r_2 N_6)$$

$$\frac{dN_6}{dt} = t_s(r_3 + rm_2 N_5 - (rm_3 + r_2)N_6)$$

where

$$r_3 = \sigma G_F r_3^0 \frac{C_i}{C_i + k_{p2}} \qquad \text{(A11)}$$

and σ is determined by Eqs. (6) in the main text and Eq. (A16) below.

Equations of the exocytosis model, simplified from [18] by setting fast steps $N_1 - N_4$ to steady state:

$$N_1 = C_{N1} N_5$$

$$N_2 = C_{N2} N_1$$

$$N_3 = C_{N3} N_2$$

$$N_4 = C_{N4} N_3$$

$$N_F = u_1 N_4 / u_2$$

$$N_R = N_F u_2 / u_3$$

$$r_2 = r_2^0 \frac{C_i}{C_I + k_{p2}} \qquad \text{(A12)}$$

$$ISR = \rho t_s u_3 N_R$$

The output of the exocytosis model vesicles/min/cell. In contrast to the first version of the model [6], σ is a unitless scale factor modifying vesicle delivery to the plasma membrane, so we need the factor ρ to convert vesicles/cell/min to μU(insulin)/mg(beta cells)/min for substitution of *ISR* into Eq. 2 for *I*. The value of ρ is approximately 90 μU/mg based on the following estimates:

1 vesicle has 9 fg of insulin [66].

A beta cell has a volume of about 3 pL [67] and weighs about 2.9 ng, so there are about 3.5×10^5 cells/mg.

1 U = 0.035 mg of insulin, giving 3.5×10^4 fg/μU.

Combining these three factors gives ρ = 90 μU/mg. However, we find that this rate, based on single-cell measurements of capacitance, gives whole-body insulin secretion that is too large. Previous reports have

said that islet secretion in vivo is 3-fold [67] and in vitro 25-fold [68] smaller than single-cell secretion. The inhibition of insulin secretion by paracrine somatostatin and by insulin itself may contribute to this. We have compromised and reduced ρ 10-fold to 9 μU/mg. With this choice, total secretion rate ($\beta ISR/V$) is in the range 100 – 550 pmol/min during an OGTT, compared to 200 – 700 pmol/min in experimental data from 7 NGT and 4 IGT subjects [69], and peak post-prandial secretion for an NGT subject is about 0.6 ng/ml/min, close to results from a mixed meal test in [70].

Table S8 Parameters for the exocytosis model

Parameter name	Value	Description	Unit
t_s	60	Unit conversion factor	*sec/min*
k_1	20	Flux	$(\mu M\ sec)^{-1}$
km_1	100	Flux	sec^{-1}
r_1	0.6	Flux	sec^{-1}
r_2^0	0.006	Flux	sec^{-1}
rm_2	0.001	Flux	sec^{-1}
r_3^0	1.205	Flux	sec^{-1}
u_1	2000	Flux	sec^{-1}
u_2	3	Flux	sec^{-1}
u_3	0.02	Flux	sec^{-1}
k_{p2}	2.3	Half activation value	μM

Dynamics of peripheral and hepatic insulin resistance. Both peripheral insulin sensitivity, S_I, and hepatic insulin resistance, $hepa_{IR}$, are modeled as decreasing exponentially to target levels tar_{SI} and tar_{hepaIR} with time constants τ_{SI} and τ_{hepaIR}, respectively.

$$\frac{dSI}{dt} = \frac{t_{min}(tar_{SI} - SI)}{\tau_{SI}} \qquad \text{(A13)}$$

$$\frac{dhepa_{SI}}{dt} = \frac{t_{min}(tar_{hepa_{SI}} - hepa_{SI})}{\tau_{hepa_{SI}}} \quad \text{(A14)}$$

Parameter adjustments for daily glucose responses. Some parameters in Tables S9 and S10 have been changed from [6] to accommodate daily glucose fluctuations.

γ–dynamics:

$$\gamma_\infty(G) = \frac{\gamma_{max}}{1+exp((G-\gamma_s)/\gamma_n)_0} \quad \text{(A15)}$$

Table S9. Parameter adjustments of γ–dynamics for daily glucose fluctuations

Parameter name	Value	Description	Unit
γ_{max}	0.4	Maximum value of γ	unitless
γ_s	100	Default value of horizontal shift	*mg/dl*
γ_n	5	Slope factor of γ_∞	unitless
γ_0	0.2	Baseline value of γ	unitless
τ_γ	3,081.6	Time constant of γ	min (2.14 *d*)

σ–dynamics:

$$\sigma_\infty(ISR, M) = \sigma_{ISR\infty}(ISR)\sigma_{M\infty}(M) + \sigma_b$$

$$\sigma_{ISR\infty}(ISR) = \frac{\sigma_{ISRmax}}{1+\sigma_{ISRk}\exp\left(-\frac{ISR-\sigma_{ISRs}}{\sigma_{ISRn}}\right)} \quad \text{(A16)}$$

$$\sigma_{M\infty}(M) = 1 - \frac{\sigma_{Mmax}}{1 + \sigma_{Mk}\exp\left(-\frac{M_\sigma - \sigma_{Ms}}{\sigma_{Mn}}\right)}$$

where $M_\sigma = M(G - G_{\sigma s})$

Table S10. Parameters of σ-dynamics for daily glucose fluctuations

Parameter name	Value	Description	Unit
σ_{ISRmax}	1.4	Maximum value of $\sigma_{ISR\infty}$	$\frac{\mu U}{\mu g \cdot d}$
σ_{ISRk}	1	Weight of $\sigma_{ISR\infty}$	
σ_{ISRs}	0.1	Horizontal shift of $\sigma_{ISR\infty}$	
σ_{ISRn}	0.1	Slope of $\sigma_{ISR\infty}$	
σ_b	0.0175	Basal sigma value	$\frac{\mu U}{\mu g \cdot d}$
σ_{Mmax}	1	Scale factor of $\sigma_{M\infty}$	
σ_{Mk}	0.2	Weight of $\sigma_{M\infty}$	
σ_{Ms}	0.2	Horizontal shift of $\sigma_{M\infty}$	$\frac{\mu U}{\mu g \cdot d}$
σ_{Mn}	0.02	Slope of $\sigma_{M\infty}$	
$G_{\sigma s}$	35	shift of glucose dependent M	*mg/dl*
τ_σ	3.598×10^5	Time constant of σ	*min* (249.9 *d*)

β–dynamics:

$$P(ISR) = P_{max} \frac{ISR^{kP}}{{\alpha_P}^{kP} + ISR^{kP}} \quad \text{(A17)}$$

$$A(M) = A_{max} \frac{M^{kA}}{{\alpha_A}^{kA} + M^{kA}}$$

Table S11. Parameters of β-dynamics for daily glucose fluctuations

1085

Parameters	Values	Description	Units (unitless if blank)
k_M	2	Exponent of metabolic rate *M*	
α_M	150	Half maximum *G* value for *M*	*mg/dl*
$kISR$	2	Exponent of insulin secretion rate *ISR*	
α_{ISR}	1.2	Half maximum *M* value for *ISR*	
P_{max}	4.55	Maximum proliferation rate	*1/day*
kP	4	Exponent of proliferation rate	
α_P	41.77	Half maximum value of *ISR* for proliferation	
A_{max}	3.11	Maximum apoptosis rate	*1/day*
kA	6	Exponent of apoptosis rate	
α_A	0.44	Half maximum value of *M* for apoptosis	
A_b	0.8	Basal apoptosis rate	*1/day*
τ_β	1.008×10^7	Time constant of β	min (7000 *d*)

1086

1087

1088

1089

1090

1091 Table S12A. Parameter values for Figs. 1 – 4

	Fig. 1 (NGT-IGT-CGT-T2D)	Fig. 2 (Maintained IGT)	Fig. 3 (NGT-IFG-CGI-T2D)	Fig. 4 (NGT-IGT-T2D)
tar_{SI}	0.1	0.1	0.5	0.03
τ_{SI}	250	250	250	150
tar_{hepaSI}	0.85	0.85	0.1	1.3
τ_{hepaSI}	250	250	250	1
γ_s	100	90	100	100

1092

1093 Table S12B. initial conditions for Figs. 1 - 4

Variables	Initial Conditions	Units (unitless if blank)
G	78.6 mg/dl	*mg/dl*
I	5.6	$\mu U/ml$
β	1533.9	*mg*
γ	-0.076	
σ	1	
S_I	0.8×10^{-4}	$ml/\mu U/min$
$hepa_{SI}$	1	
N_5	60.2	
N_6	443.4	

1094

1095 Table S13. Parameter values for Fig. 8A

1096

	High-dose TZD	High-dose metformin
Initiation of drug therapy	4.25 years	4.25 years
S_I	0.1→0.25	0.1→0.1

$hepa_{SI}$	0.85→0.85	0.85→1.5
τ_{SI}	15 (days)	250 (days)
τ_{hepaSI}	250 (days)	15 (days)

Table S14. Parameter values for Fig. 8B

	High-dose metformin	High-dose TZD
Initiation of drug therapy	4.25 years	4.25 years
S_I	0.5→0.5	0.5→0.65
$hepa_{SI}$	0.1→0.5	0.1→0.1
τ_{SI}	250 (days)	15 (days)
τ_{hepaSI}	15 (days)	250 (days)

Table S15. Parameter values for Fig. 8C

	Low-dose TZD	Low-dose metformin
Initiation of drug therapy	2.43 years	2.43 years
S_I	0.1→0.2	0.1→0.1
$hepa_{SI}$	0.85→0.85	0.85→1.25
τ_{SI}	15 (days)	250 (days)
τ_{hepaIR}	250 (days)	15 (days)

Table S16. Parameter values for Fig. 8D

	Low-dose metformin	Low-dose TZD
Initiation of drug therapy	2.43 years	2.43 years
S_I	0.5→0.5	0.5→0.6

$hepa_{SI}$	0.1→0.25	0.1→0.1
τ_{SI}	250 (days)	15 (days)
τ_{hepaIR}	15 (days)	250 (days)

1104

Fig. 1

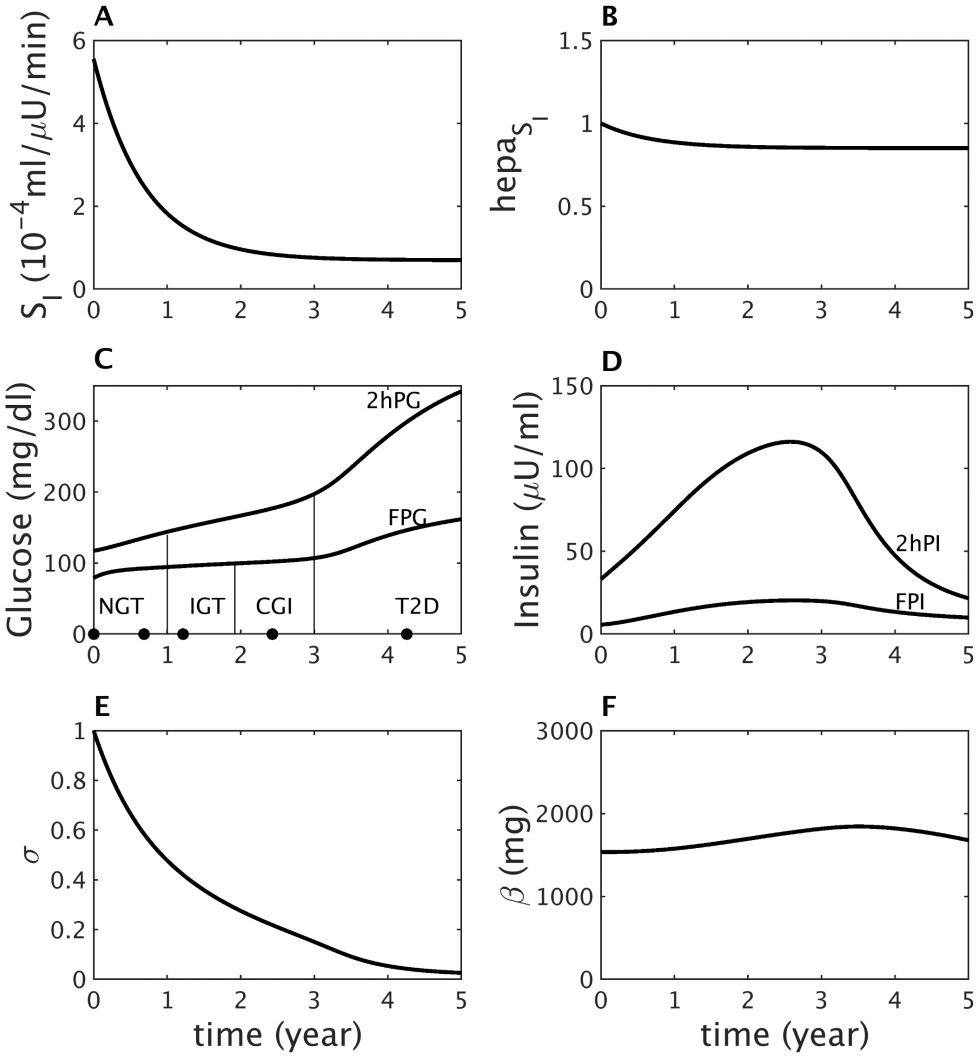
A
B
C
D
E
F
S_I (10^{-4}ml/μU/min)
$hepa_{S_I}$
Glucose (mg/dl)
2hPG
FPG
NGT
IGT
CGI
T2D
Insulin (μU/ml)
2hPI
FPI
σ
β (mg)
time (year)
time (year)

Fig. 2

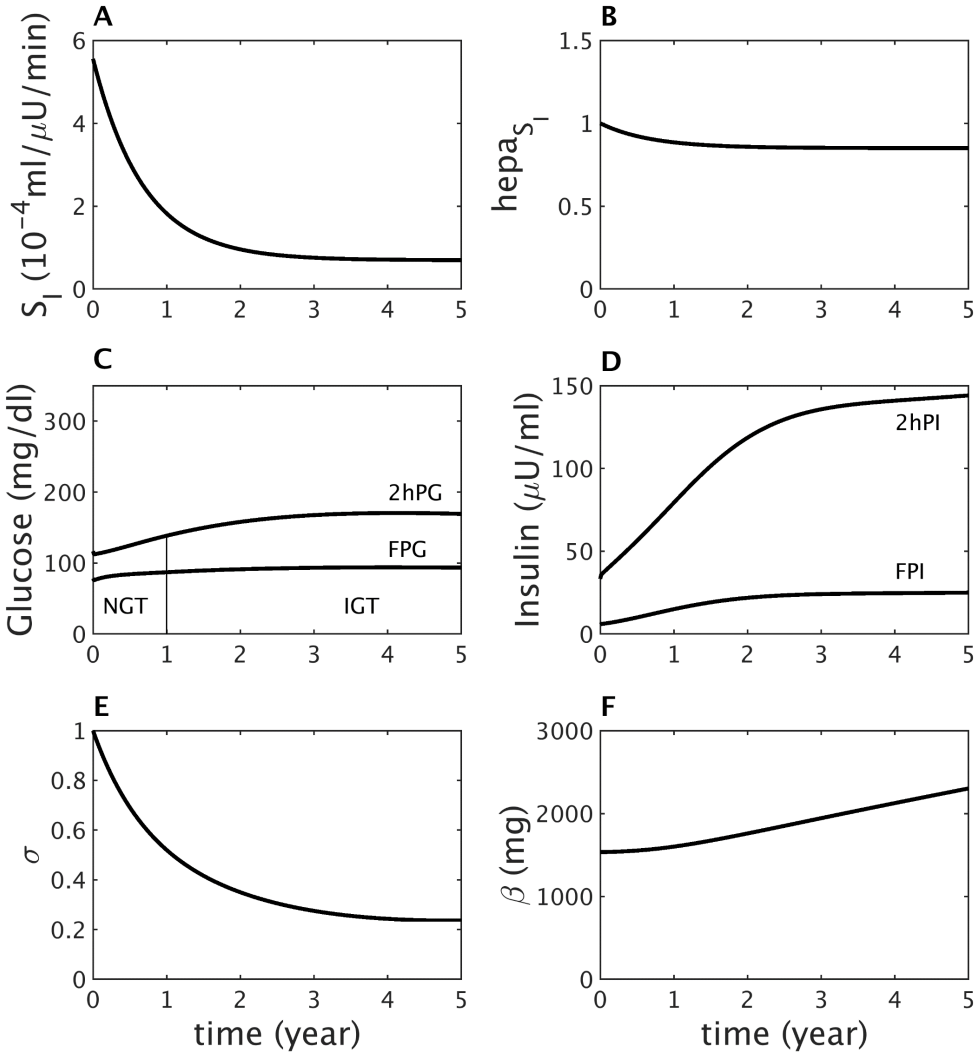
A
S_I (10^{-4}ml/μU/min)
B
$hepa_{S_I}$
C
Glucose (mg/dl)
2hPG
FPG
NGT
IGT
D
Insulin (μU/ml)
2hPI
FPI
E
σ
time (year)
F
β (mg)
time (year)

Fig. 3

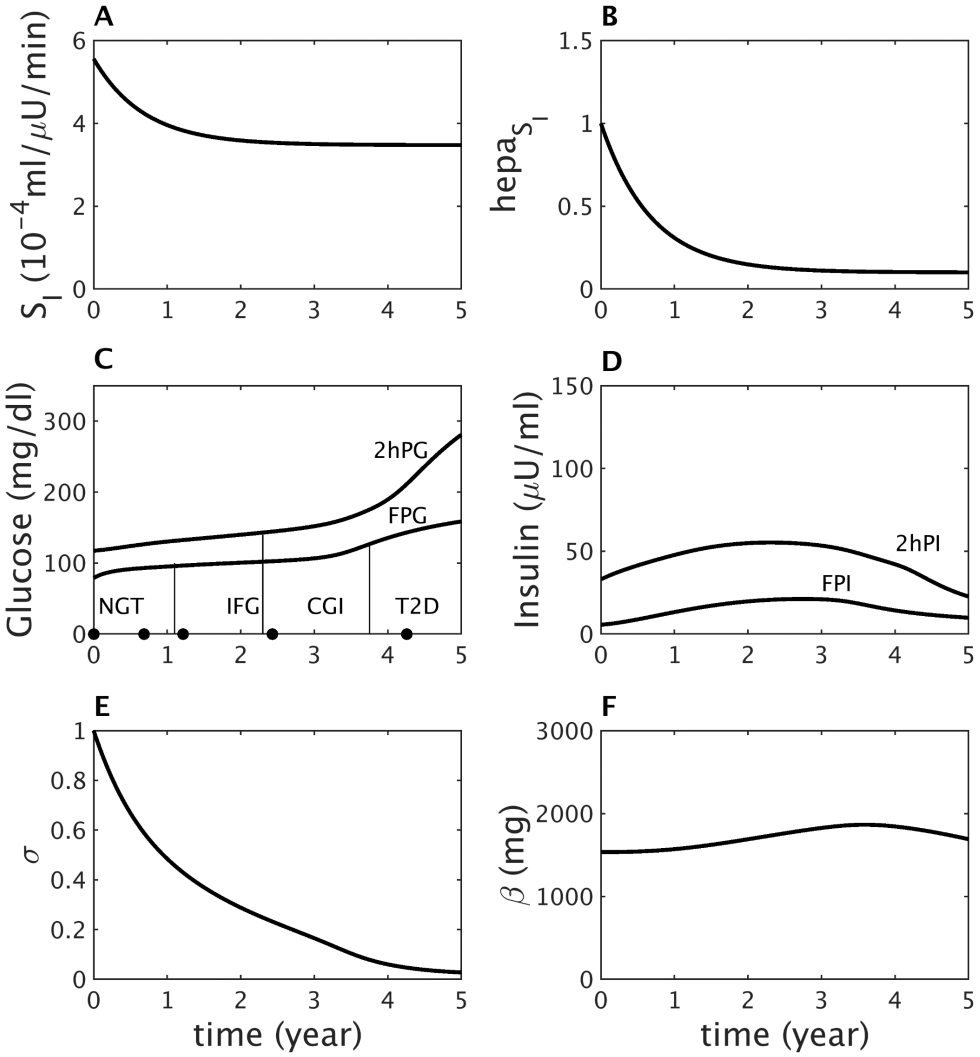
A
B
C
D
E
F
S_I (10^{-4}ml/μU/min)
hepa$_{S_I}$
Glucose (mg/dl)
2hPG
FPG
NGT
IFG
CGI
T2D
Insulin (μU/ml)
2hPI
FPI
σ
β (mg)
time (year)
time (year)

Fig. 4

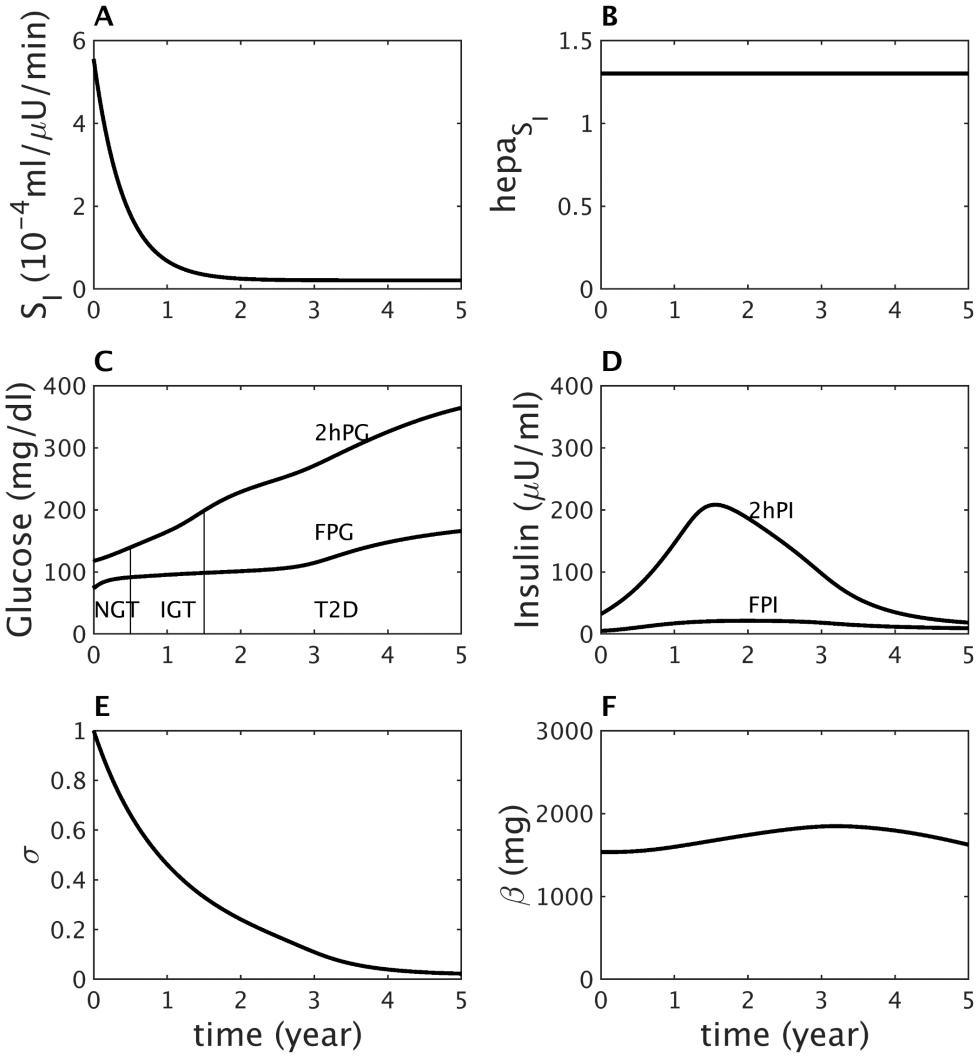
A
B
C
D
E
F
S_I (10^{-4}ml/μU/min)
hepa$_{S_I}$
Glucose (mg/dl)
2hPG
FPG
NGT
IGT
T2D
Insulin (μU/ml)
2hPI
FPI
σ
β (mg)
time (year)
time (year)

Fig. 5

A

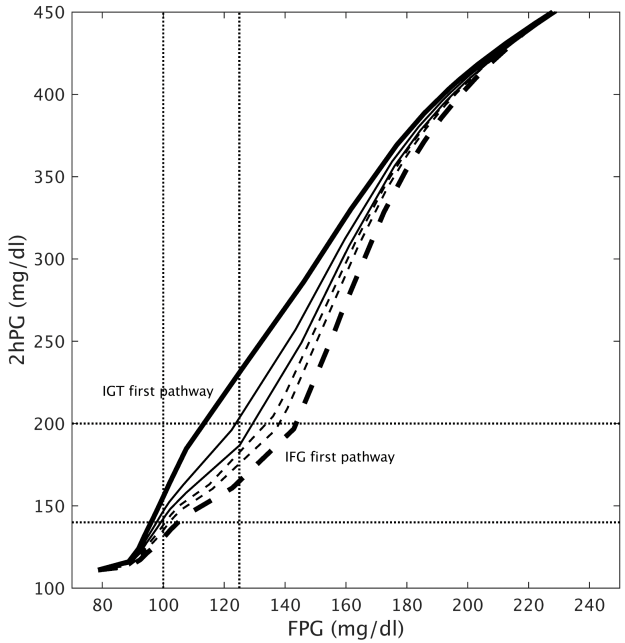
2hPG (mg/dl)
FPG (mg/dl)
IGT first pathway
IFG first pathway
100
150
200
250
300
350
400
450
80
100
120
140
160
180
200
220
240

B

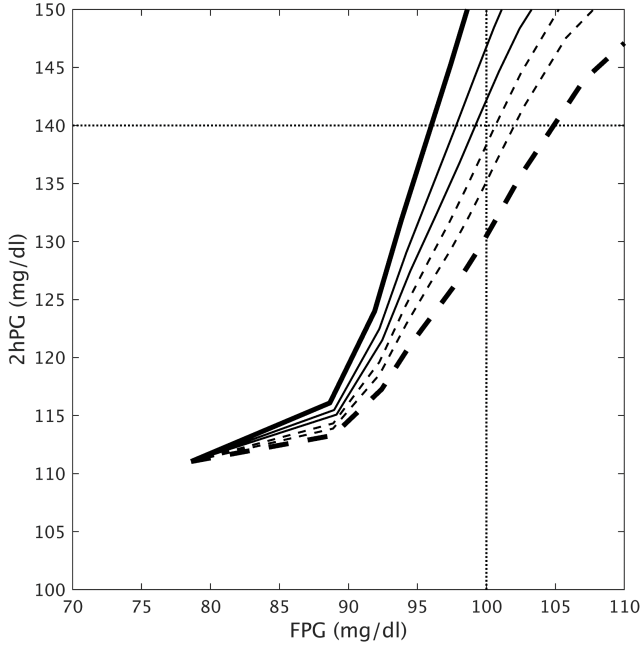
2hPG (mg/dl)
FPG (mg/dl)
100
105
110
115
120
125
130
135
140
145
150
70
75
80
85
90
95
100
105
110

Fig. 6

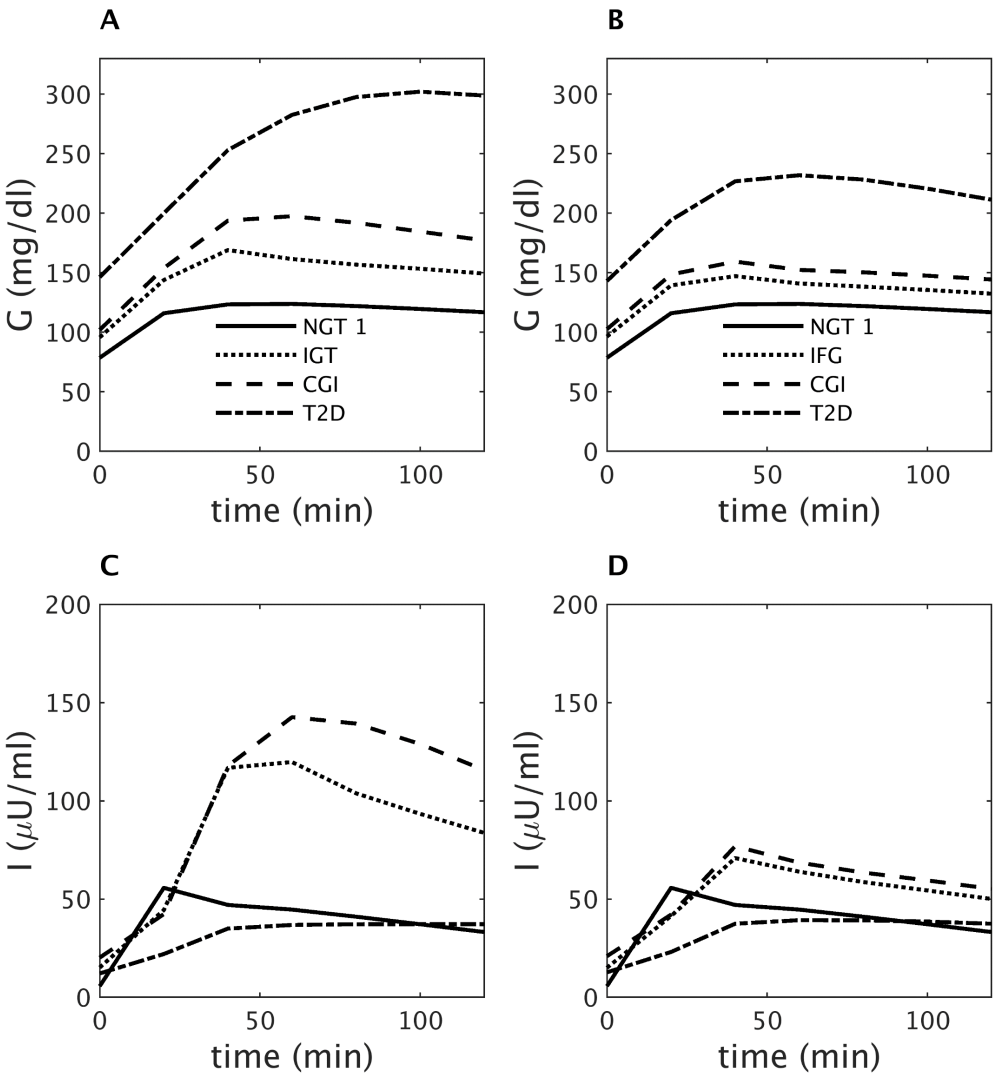
A
B
C
D
G (mg/dl)
I (μU/ml)
time (min)
NGT 1
IGT
IFG
CGI
T2D
0
50
100
150
200
250
300

Fig. 7

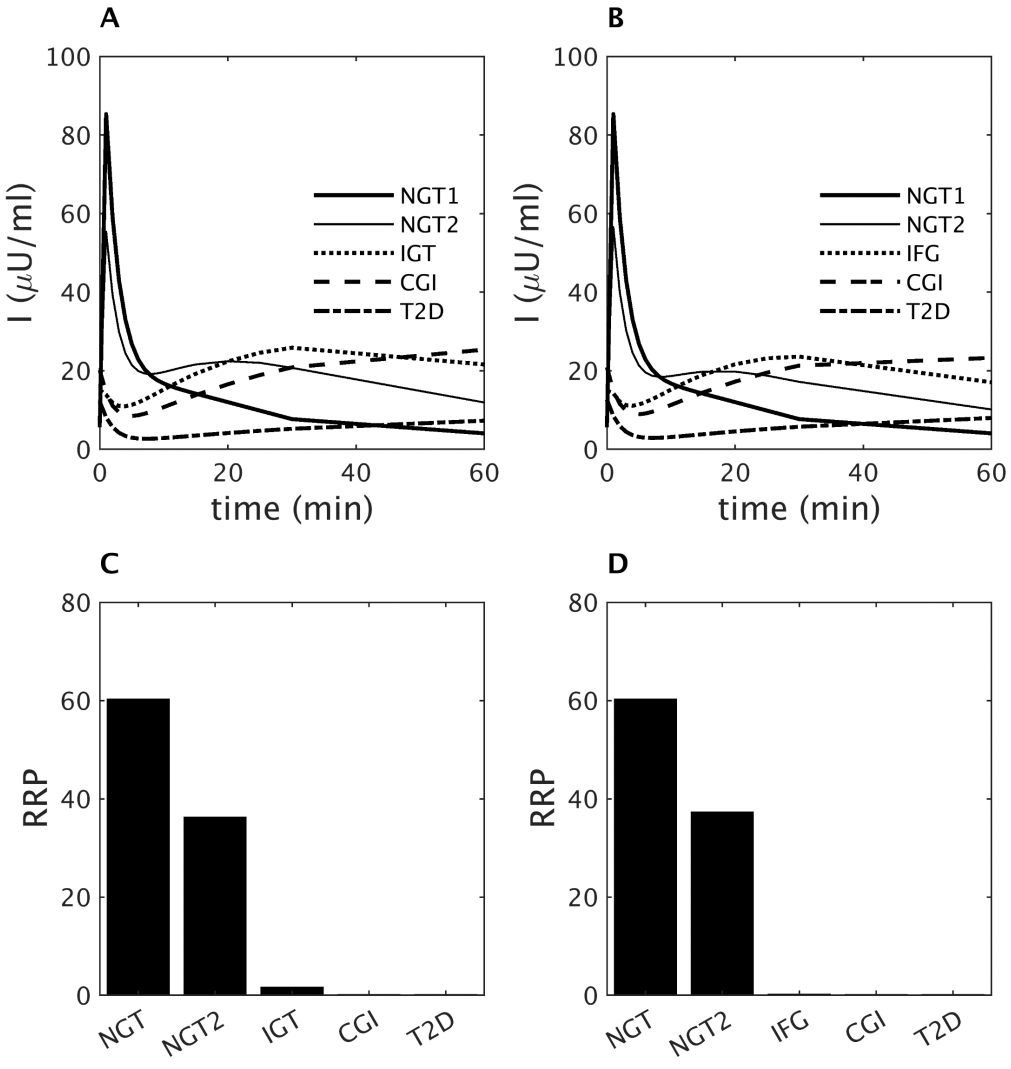
A
B
C
D
I (μU/ml)
time (min)
NGT1
NGT2
IGT
IFG
CGI
T2D
RRP
NGT
NGT2
IGT
IFG
CGI
T2D
0
20
40
60
80
100

Fig. 8

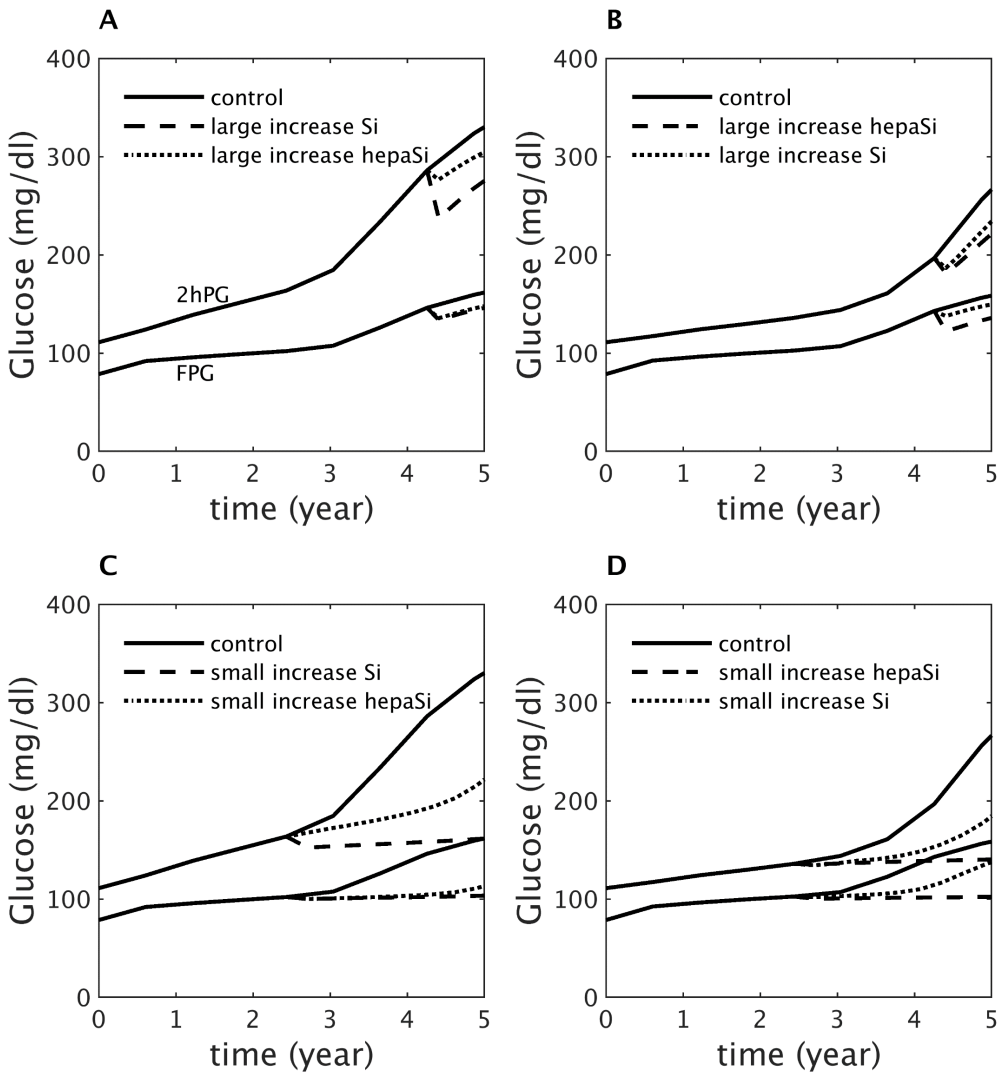
A
B
C
D
Glucose (mg/dl)
time (year)
control
large increase Si
large increase hepaSi
small increase Si
small increase hepaSi
2hPG
FPG
0
100
200
300
400
0
1
2
3
4
5

Fig. A1

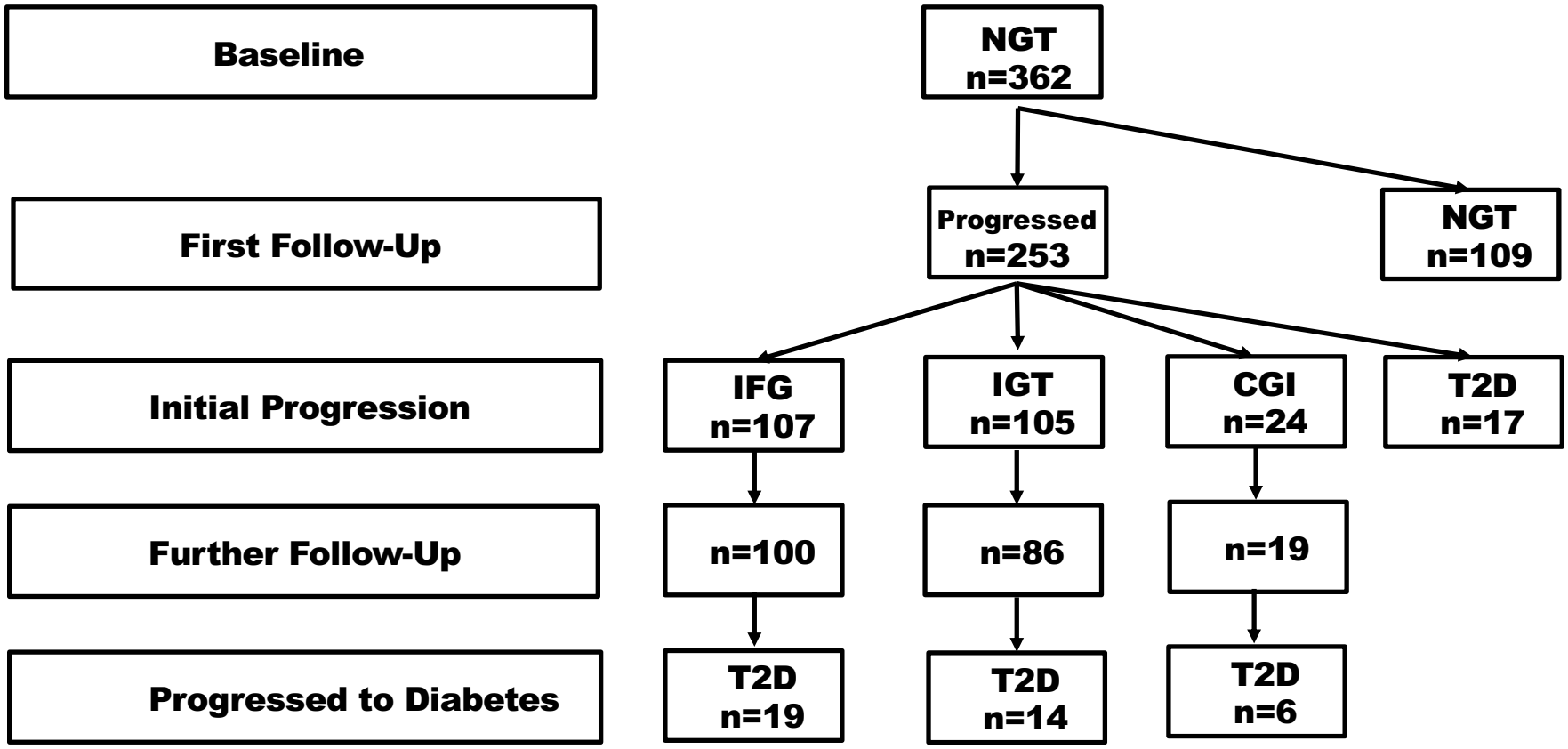
Baseline
First Follow-Up
Initial Progression
Further Follow-Up
Progressed to Diabetes
NGT n=362
Progressed n=253
NGT n=109
IFG n=107
IGT n=105
CGI n=24
T2D n=17
n=100
n=86
n=19
T2D n=19
T2D n=14
T2D n=6

Fig. A2

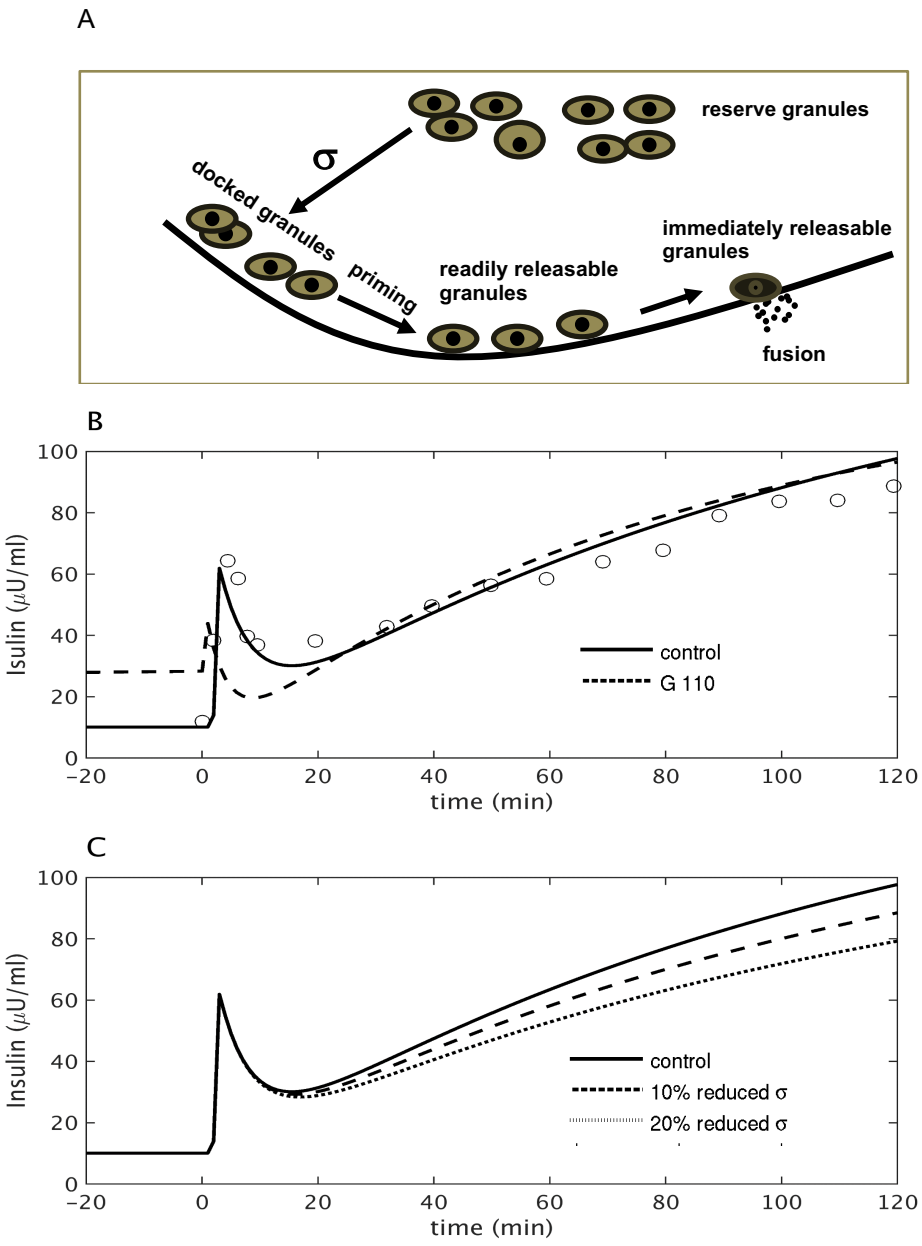
A
reserve granules
σ
docked granules
priming
readily releasable granules
immediately releasable granules
fusion
B
Isulin (μU/ml)
time (min)
control
G 110
C
Insulin (μU/ml)
time (min)
control
10% reduced σ
20% reduced σ

Fig. A3

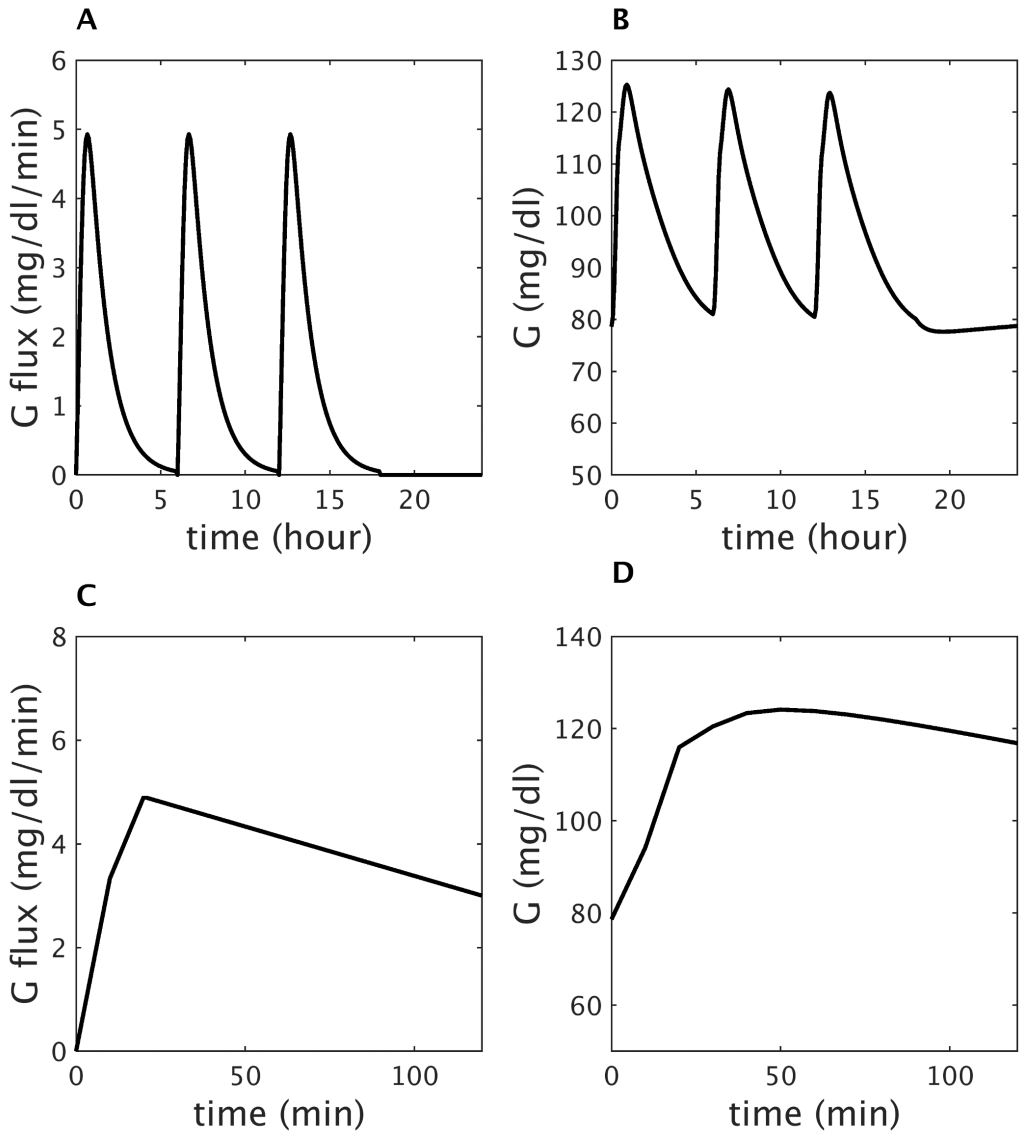
A
G flux (mg/dl/min)
time (hour)
B
G (mg/dl)
time (hour)
C
G flux (mg/dl/min)
time (min)
D
G (mg/dl)
time (min)

Fig. A4

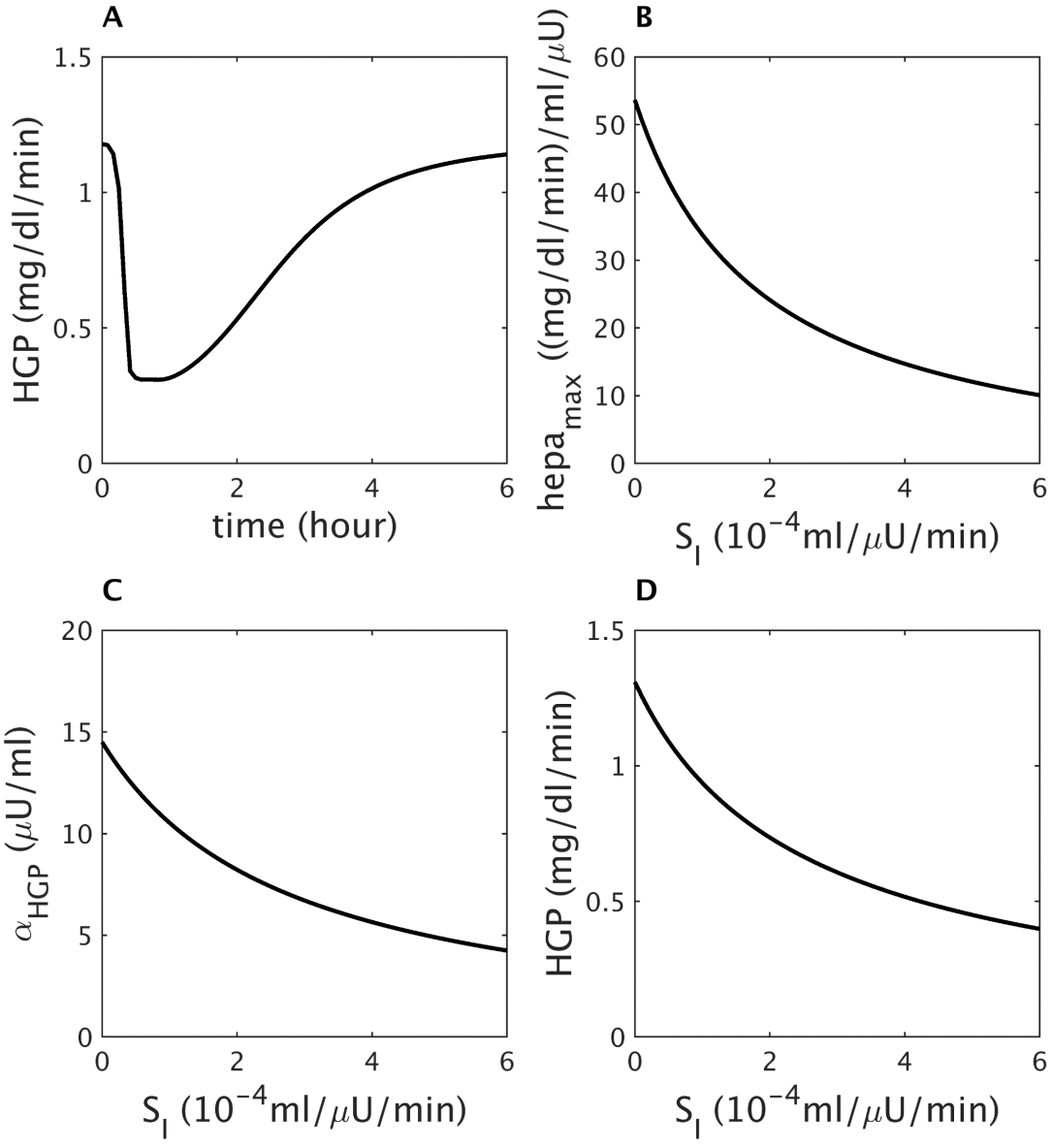
A
1.5
1
0.5
0
HGP (mg/dl/min)
0
2
4
6
time (hour)
B
60
50
40
30
20
10
0
hepa$_{max}$ ((mg/dl/min)/ml/μU)
0
2
4
6
S$_I$ (10^{-4}ml/μU/min)
C
20
15
10
5
0
α_{HGP} (μU/ml)
0
2
4
6
S$_I$ (10^{-4}ml/μU/min)
D
1.5
1
0.5
0
HGP (mg/dl/min)
0
2
4
6
S$_I$ (10^{-4}ml/μU/min)

Fig. A5

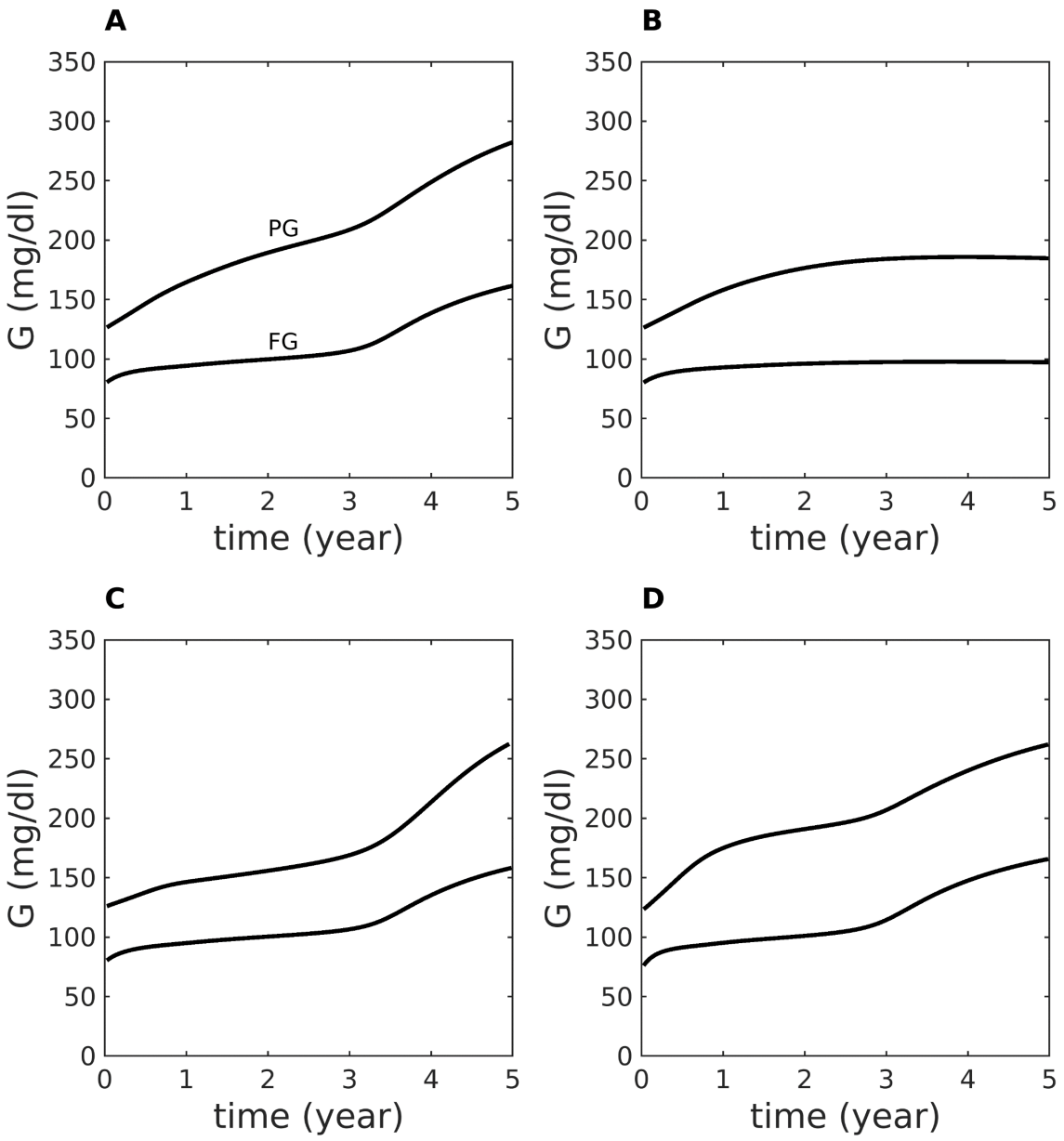

Fig. A6

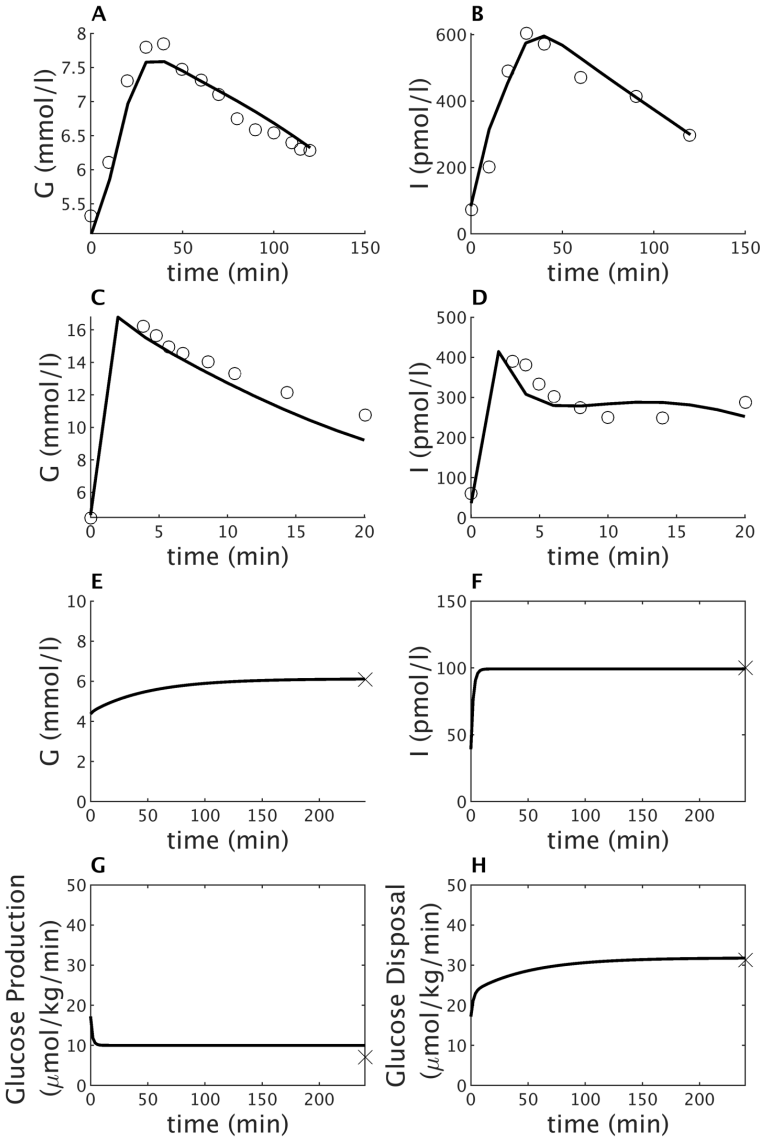
A
G (mmol/l)
time (min)
B
I (pmol/l)
time (min)
C
G (mmol/l)
time (min)
D
I (pmol/l)
time (min)
E
G (mmol/l)
time (min)
F
I (pmol/l)
time (min)
G
Glucose Production
(μmol/kg/min)
time (min)
H
Glucose Disposal
(μmol/kg/min)
time (min)

Fig. A7

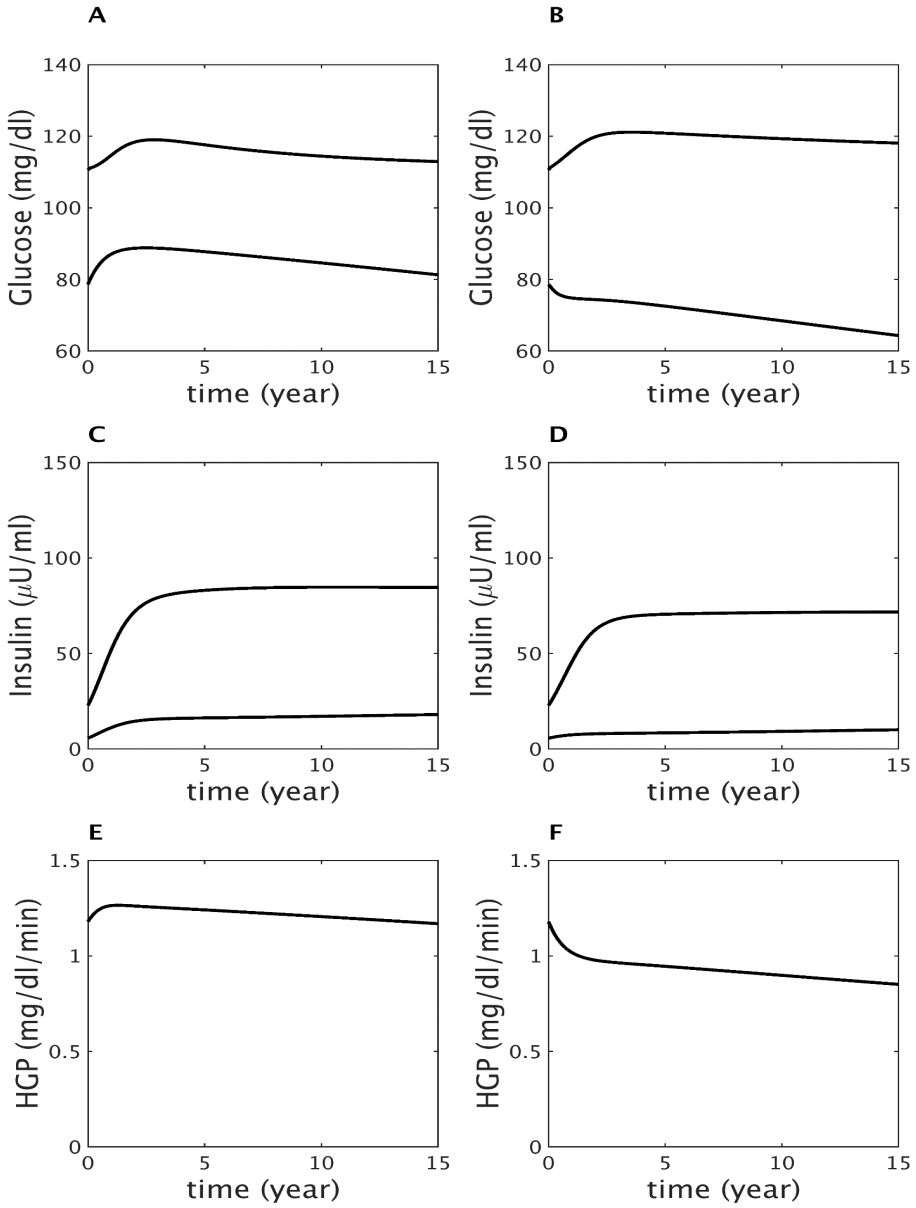
A
B
C
D
E
F
Glucose (mg/dl)
Insulin (μU/ml)
HGP (mg/dl/min)
time (year)
140
120
100
80
60
150
50
0
1.5
1
0.5
0
5
10
15